TMX 2.

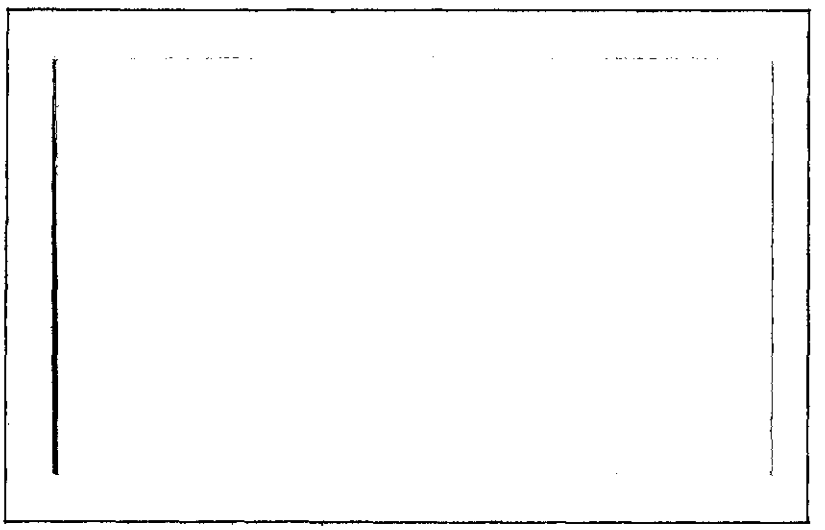

METALS RESEARCH LABORATORY

CARNEGIE INSTITUTE OF TECHNOLOGY

Carnegie-Mellon University

PITTSBURGH, PENNSYLVANIA

N75-15773

National Aeronautics and Space Administration
Research Grant NGR 39-087-047

The Effect of Microstructure on the Fracture Toughness of Titanium Alloys

by

R. H. Van Stone,* J. R. Low, Jr.,*
and
J. L. Shannon, Jr.**

* Department of Metallurgy and Materials Science
Carnegie-Mellon University
Pittsburgh, Pennsylvania 15213

** National Aeronautics and Space Administration
Lewis Research Center
Cleveland, Ohio 41135

NASA Technical Report No. 2-Ti
December 1974

This investigation was made possible by a Research Grant from the National Aeronautics and Space Administration

This is the annual report on National Aeronautics and Space Administration Grant 39-087-047 for the period from September 25, 1973 to November 30, 1974. The principal investigator was Professor John R. Low, Jr. and the NASA Technical Officer was Mr. W. D. Klopp, Head, Materials Development Section at NASA Lewis Research Center.

ABSTRACT

This report describes the progress made in an investigation of the effect of microstructure on the fracture mechanism and fracture toughness of the α titanium alloy Ti-5Al-2.5Sn and the metastable β titanium alloy Beta III (Ti-11.5Mo-6Zr-4.5Sn). The Ti-5Al-2.5Sn material being studied is from normal and extra low interstitial grade plates which have been either air-cooled or furnace-cooled from an 815°C (1500°F) annealing treatment. Tensile and plane strain fracture toughness tests have been performed at 295°K (72°F), 77°K (-320°F), and 20°K (-423°F). The fracture mode is always dimpled rupture, but the morphology changes from classical, equiaxed dimples to long shallow ones as the toughness is decreased as a result of reduced alloy purity, lower testing temperature, or slower cooling rate from the annealing temperature. Beta III is being studied in α-aged and ω-aged plates which were heat treated to similar strength levels. Tensile and plane strain fracture toughness tests have been performed at room temperature on the α-aged material and the fracture mode is classical dimpled rupture. In tensile specimen fractures, the dimples are of one size, but fractographs from fracture toughness specimens show populations of large and small dimples. The microstructure and fracture mechanisms of these alloys are being studied using optical metallography, electron microscopy, microprobe analyses, and texture pole figures. Suggestions are made on how the microstructure affects the fracture mechanisms and fracture toughness of these alloys. The types of experiments which are going to be carried out during the remainder of this investigation are also described.

INTRODUCTION

Titanium alloys are widely used in aerospace and hydrospace structures because of their high strength-to-weight ratios but very little research has been completed to directly link the microstructure to the fracture mechanism which, in turn, affects the fracture toughness. This report describes the work completed to date on an investigation of the effect of microstructure on the fracture mechanism and fracture toughness of titanium alloys. The alloys chosen for this study are the α alloy Ti-5Al-2.5Sn and the metastable β alloy Ti-11.5Mo-6Zr-4.5Sn, known as Beta III. These alloys are being studied so that suggestions can be made on how to modify their composition and microstructure so as to improve their fracture toughness without significant loss in strength. This investigation may also help to understand the relationship between microstructure and fracture toughness in the more complex α + β titanium alloys such as Ti-6Al-4V.

Ti-5Al-2.5Sn is used for liquid hydrogen temperature (20°K or -423°F) service in space applications where high strength-to-weight ratios and fracture toughness are essential. Materials capable of cryogenic service, like Ti-5Al-2.5Sn, may also play an important role in the development of liquid hydrogen as a commercial energy source.

Metastable β titanium alloys like Beta III are useful in a broad range of ambient temperature structural applications. They exhibit deep hardenability and can be hot worked, cold worked, and welded in the solution treated condition. In the aged condition, these alloys have strengths which approach those of quenched and tempered low alloy steels, but the density of Beta III is 35 percent less than the density of steel. For many applications, they may challenge aluminum alloys and steels for major structural components in aircraft because of the overall savings in weight.

This report gives a condensed review of the literature on these alloys and describes the progress of the present investigation. Results which have been reported previously[1] will be summarized in the appropriate sections of the report.

LITERATURE REVIEW

The literature on these alloys has been reported in detail previously[1] and only highlights of that review will be given.

Ti-5Al-2.5Sn is based on the binary titanium-aluminum system. In that system, a long range ordered phase (α_2) which has a composition close to that of Ti_3Al has been observed in alloys with aluminum contents as low as 7.7 weight percent.[2, 3] In 6 weight percent alloys, electron diffraction patterns have shown spots which can be indexed as α_2 but no particles could be imaged using dark field microscopy.[3] It has been suggested that short range order exists in titanium-4 weight percent aluminum alloys.[3]

Deformation in titanium-aluminum alloys occurs by slip and twinning. Increases in strength level, whether caused by increased aluminum content, increased interstitial (mainly oxygen) levels, or decreased testing temperature, results in more planar dislocation arrays.[4-7] The amount of twinning observed[13] is increased by lowering the deformation temperature but is reduced by increasing the aluminum or oxygen contents.[6-8]

Ti-5Al-2.5Sn has a microstructure of α grains with a second phase present which is especially notable in alloys with higher iron contents.[9] Several investigators[10, 11] have looked for α_2 precipitation in this alloy using electron microscopy, but no evidence of its presence could be found. Shannon and Brown[12] investigated the effects of alloy purity, heat treatment, and processing variables on the mechanical properties of annealed Ti-5Al-2.5Sn sheet. The strengths of their alloys at liquid hydrogen temperature (20°K or -423°F) were twice those measured at room temperature. The toughness, as measured by the strength of sharply notched sheets, decreased suddenly near 77°K (-320°F) for extra low interstitial (ELI) grades; but the notched strength for normal interstitial alloys, which also have higher iron contents, dropped suddenly near 200°K (-100°F). It was noted that ELI sheets which

had been furnace cooled from the annealing treatment had much lower notched strengths than air-cooled material. Shannon and Brown suggested that this was the effect of ordering, but no evidence was presented to show that ordering existed.

Beta III (Ti-11.5Mo-6Zr-4.5Sn) is an alloy based on the titanium-molybdenum phase diagram. Zirconium is added to aid molybdenum melting during the melting process[13] and zirconium and tin reduce the volume fraction of the embrittling ω phase which form during low temperature aging.[14] When Beta III is aged above 455°C (850°F), the hexagonal close packed α phase precipitates in the body centered cubic β matrix. Aging below that temperature results in ω precipitation and is accompanied by drastic reductions in tensile ductility and fracture toughness.[15] For structural applications, Beta III is solution treated slightly below or above the β transus ($\alpha+\beta/\beta$ solvus line), water quenched, and aged to precipitate the α phase. The strength, fracture toughness, and stress corrosion properties of α-aged Beta III solution treated just below the β transus are superior to those treated in the β phase field. Guernsey, Petersen, and Froes[16] have attributed the poorer properties of Beta III solution treated above the β transus to the precipitation of large amounts of primary α which forms at the β grain boundaries during cooling from the solution treatment temperature. This alloy fails by dimpled rupture in the solution treated, α-aged, and ω-aged conditions,[15] but no void initiation sites have been identified.

SCOPE OF THIS INVESTIGATION

Ti-5Al-2.5Sn alloys are being studied in four conditions. Plate material of two grades, normal interstitial and extra low interstitial (ELI), received a mill anneal at 815°C (1500°F) followed by either air or furnace cooling. The tensile properties, flow curves, and K_{Ic} for all four conditions have been determined at 295°K (72°F), 77°K (-320°F), and 20°K (-423°F). The fracture modes have been determined for most of these conditions using transmission electron microscope replicas taken from the fracture surfaces of both tensile and K_{Ic} specimens. The fracture mode at liquid nitrogen temperature (77°K) was similar to the mode at the liquid hydrogen temperature (20°K). Thus, the fracture mechanisms will be studied at 77°K to yield information which should apply equally to the improvement of the 20°K fracture toughness.

Beta III is being studied using a sub-β transus solution treated plate which was aged to precipitate either the α or ω phase. The α-aging sequence was a typical commercial heat treatment of 496°C (925°F) for eight hours and the ω-aging was done at 371°C (700°F) for the time required to produce a strength level as close as possible to the α-aged material. The tensile properties, flow curves, and K_{Ic} will be determined at 295°K (72°F) and the fracture modes in both specimen geometries will be identified from transmission electron microscope replicas.

The fracture mechanism of Ti-5Al-2.5Sn at 77°K and Beta III at 295°K will be investigated through the use of quantitative fractography and metallographic sectioning. Tensile and K_{Ic} specimens will be strained to several levels short of final rupture, when this is possible. These specimens will be sectioned to study the fracture mechanism as it develops in thick sections. This approach has been very successful in determining the role

microstructure plays in the fracture process in aluminum alloys[17] and steels[18] and it is hoped that similar results can be achieved in the study of titanium alloys.

This report describes the progress of this investigation to date.

MATERIALS AND MICROSTRUCTURE

A. Ti-5Al-2.5Sn

Ti-5Al-2.5Sn is being investigated in both normal interstitial and extra low interstitial (ELI) grades which were either air-cooled or furnace-cooled from an 815°C (1500°F) mill annealing treatment. A 2.5 cm. (1 inch) thick plate of each condition was supplied to the NASA Lewis Research Center by Titanium Metals Corporation of America (TMCA) and portions of this material were made available for this investigation. The air-cooled and furnace-cooled plates of each grade were manufactured from the same heat to avoid minor composition variations. The cooling rates from the annealing treatment were not measured, but were estimated from experimental data on other titanium plates using the same equipment.[19] The estimated cooling rates are 800°C/hr. (1440°F/hr.) for the air-cooled plates and 15°C (27°F/hr.) for the furnace-cooled plates.

Chemical analyses of the plates were determined by Ti Tech International of Ponona, California. The results of their check analyses, the compositional specifications, and the heat analyses of the α-alloys are given in Table I. The compositions are within the specifications and comparison of the check analyses of the same grade show variations that are within the maximum error of the check analysis. The major differences between the normal interstitial and ELI grades are amounts of iron and the interstitial oxygen, carbon, nitrogen, and hydrogen. Comparison of the two grades shows that the iron content is approximately two times greater and the oxygen levels are about three times greater in the normal interstitial material. Throughout this report, the designation of purity level will be the interstitial content which is the convention in the titanium industry. One must note, however, that the non-interstitial iron content also varies with alloy purity and may have a large effect on the fracture toughness.

TABLE I

CHEMICAL ANALYSES OF Ti - 5 Al - 2.5 Sn ALLOYS
(Weight Percent)

	Al	Sn	Fe	Mn	O	C	N	H
Normal Int. Specification	4.0/6.0	2.0/3.0	0.50 Max	0.30 Max	0.20 Max	0.15 Max	0.07 Max	0.003/0.020
Normal Int. Heat Analysis	5.1	2.5	0.28	0.006	0.16	0.024	0.023	0.009
Normal Int., AC* Check Analysis	5.22	2.47	0.300	0.002	0.164	0.0140	0.0163	0.0072
Normal Int., FC† Check Analysis	5.24	2.47	0.270	0.002	0.169	0.0120	0.0172	0.0042
ELI Specification	4.7/5.6	2.0/3.0	0.1/0.2	--	0.12 Max	0.08 Max	0.05 Max	0.0125 Max
ELI Heat Analysis	5.0	2.6	0.16	0.006	0.086	0.023	0.010	0.006
ELI, AC * Check Analysis	5.09	2.44	0.140	0.002	0.054	0.0057	0.0098	0.0056
ELI, FC † Check Analysis	5.10	2.47	0.145	0.002	0.052	0.0041	0.0098	0.0050
Maximum Error in Check Analysis	0.200	0.150	0.010	0.0005	0.010	0.0010	0.0010	0.0010

* Air Cooled
† Furnace Cooled

Optical micrographs of the microstructure of these alloys (revealed with an $HF-HNO_3-H_2O$ etch of the ratio 1:2:50) are shown in Figure 1. In that figure, the rolling direction is vertical and the transverse direction is horizontal. The α grains are equiaxed and there is no evidence of a Widmanstatten structure. The grain size is about 40 μm in the normal interstitial alloys and about 70 μm in the ELI alloys.

The second phase which can be observed in the background of Figure 1 is shown in more detail in Figure 2. In these micrographs, the rolling direction is vertical and the thickness direction is horizontal. In the ELI alloys this phase is about 2 μm in size and is distributed randomly. In the normal interstitial material, the second phase is about 5 μm in size, has a larger volume, and appears to have formed between Widmanstatten plates earlier in the processing history. Many papers have reported a second phase with a similar appearance as iron-stabilized β, largely without proof. Curtis, Boyer, and Williams,[10] on the other hand, have identified the β phase in normal interstitial Ti-5Al-2.5Sn using thin foil transmission electron microscopy. Christian, Hurlich, Chaffey, and Watson[9] have shown that in Ti-5Al-2.5Sn alloys a second phase which is observed in the optical microscope has a larger volume fraction as the alloy iron content increases, implying the phase is rich in iron. X-ray diffractometer traces from the α alloys used in this investigation have been unable to clearly resolve any β peaks due to the large α peaks. As a result, this phase will be identified with microprobe analysis techniques and selected area diffraction on thin foil transmission electron microscopy specimens.

A microprobe specimen was prepared containing material from the four Ti-5Al-2.5Sn alloys as well as standards of titanium, aluminum, tin, and iron. An ARL microprobe operated at 20 kv was used to determine the composition of the matrix of both air-cooled alloys at three positions and

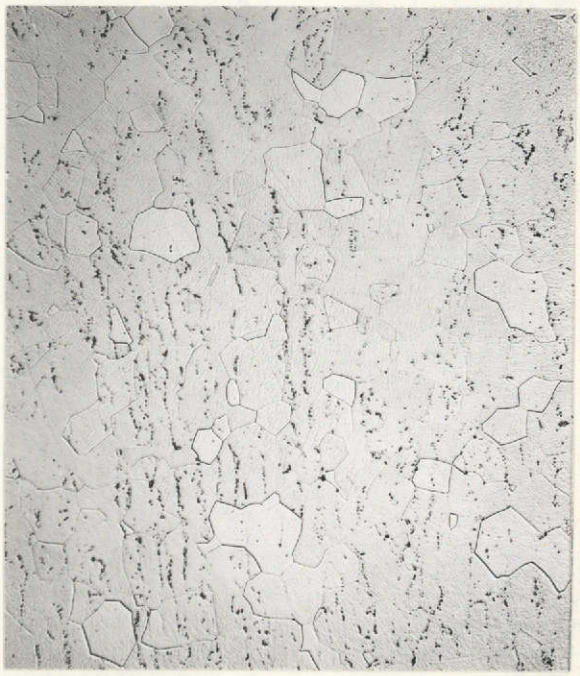

ELI, Air Cooled

ELI, Furnace Cooled

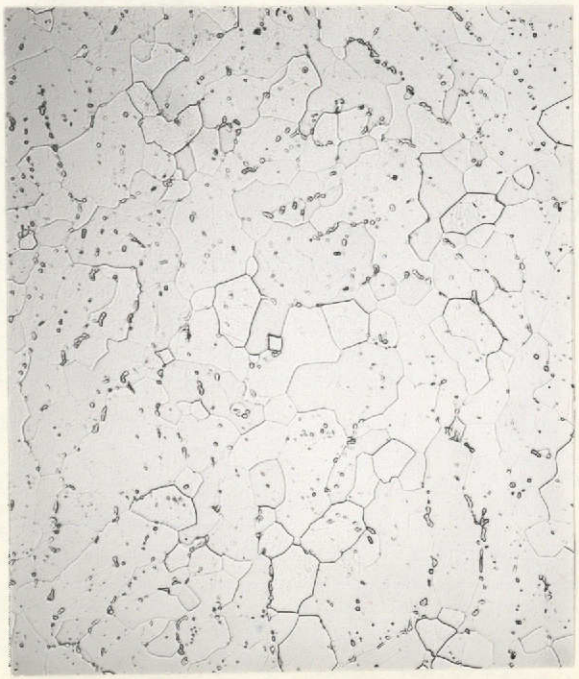

Normal Interstitial, Air Cooled

Normal Interstitial, Furnace Cooled

200μm

Figure 1. Micrographs of the Ti-5Al-2.5Sn alloys. (The rolling direction is vertical and the transverse direction is horizontal.)

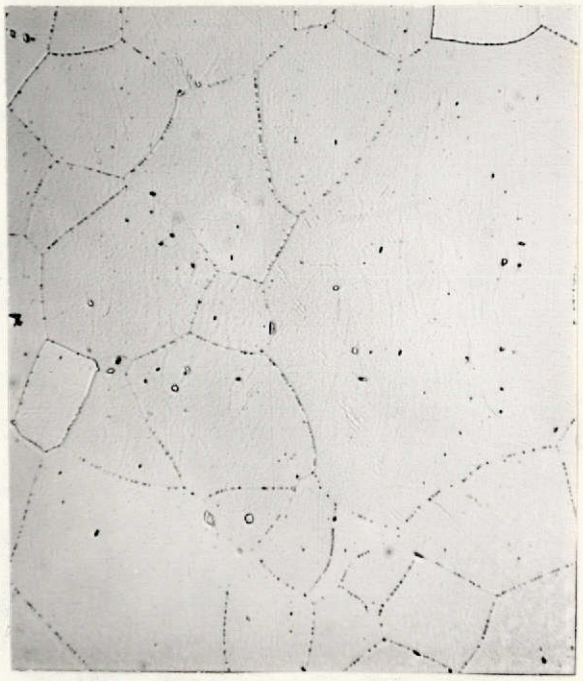

ELI, Air Cooled

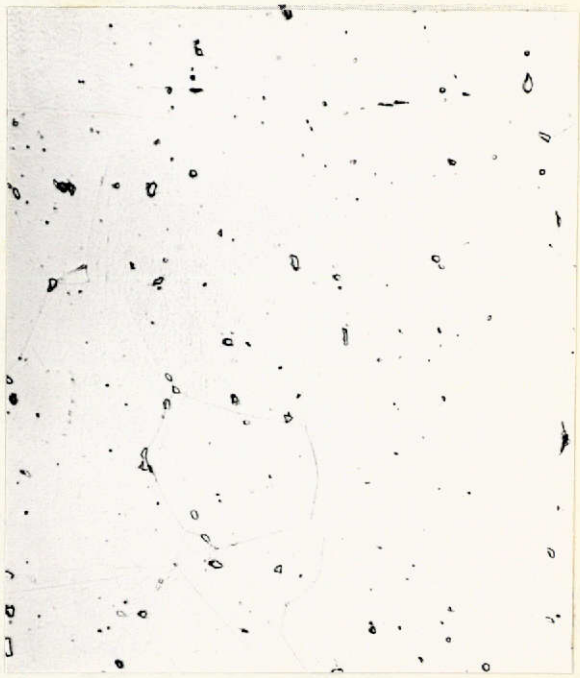

ELI, Furnace Cooled

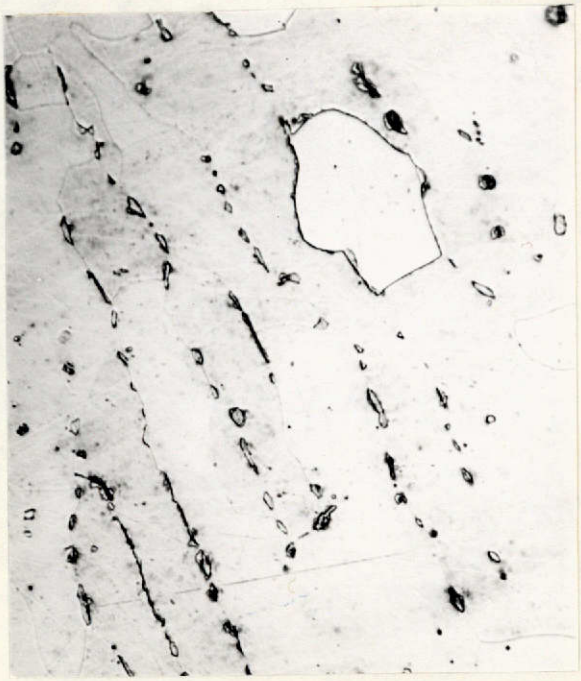

Normal Interstitial, Air Cooled

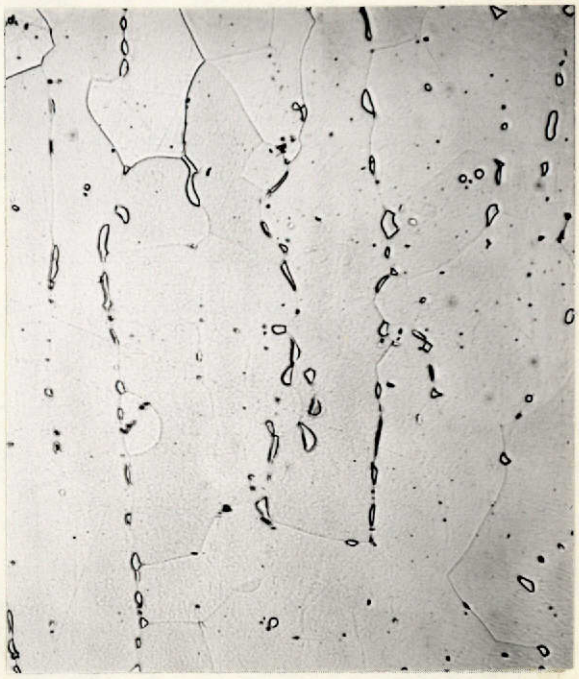

Normal Interstitial, Furnace Cooled

50μm

Figure 2. Micrographs showing the dispersed second phase in the Ti-5Al-2.5Sn alloys. (The rolling direction is vertical and the thickness direction is horizontal.)

the composition of seven of second-phase particles in the air-cooled, normal interstitial material. The aluminum and iron contents were determined from K_α radiation and the tin level was determined from L_α radiation. All three intensities were measured simultaneously. The compositions were determined by comparing the x-ray intensity of each element to the intensity of the standard and making corrections for background intensity, detector dead time, backscatter, ionization-penetration, absorbtion, and florescence through use of a computer program.[20] Aluminum had the largest correction factor which was typically 1.6 and was largely due to the absorbtion correction.

The results of the microprobe analyses are listed in Table II along with the bulk compositions of the alloys as taken from Table I. For the ELI alloy, the microprobe analysis of the matrix is in good agreement with the bulk analysis indicating the microprobe analysis is accurate. The composition determined for the second phase in the ELI material is rich in iron but is not reported because the estimated beam diameter (2.5 μm) and the depth of the material which was analyzed (2 μm)[20] are similar to the size of the particles in the ELI plate so it is likely that material outside the particle was considered in that analysis.

The matrix of the normal interstitial alloy was depleted of iron and enriched in aluminum while the particle was iron-rich and depleted in aluminum. Tin did not greatly partion between the second phase and the matrix. The second phase which was observed metallographically has an iron content of the order of 6.5 weight percent and thus its description as iron-stabilized β is at least half correct. If one assumes the iron-rich phase is β, the trends in the composition of aluminum and tin can be predicted from the Ti-Al[2, 3] and Ti-Sn[21] binary phase diagrams.

TABLE II

RESULTS OF MICROPROBE ANALYSES ON Ti-5Al-2.5Sn ALLOYS

(Values are given in weight percent and indicate the mean and the standard deviation)

Alloy and Microstructural Feature	Al	Sn	Fe
Ti-5Al-2.5Sn, ELI Air Cooled			
Matrix	5.28 ± 0.56	2.77 ± 0.36	0.18 ± 0.02
Bulk Analysis*	5.09	2.44	0.14
Ti-5Al-2.5Sn, Normal Interstitial, Air Cooled			
Matrix	5.67 ± 0.14	2.48 ± 0.19	0.09 ± 0.00+
Particle	3.00 ± 0.24	3.41 ± 0.46	6.54 ± 0.54
Bulk Analysis*	5.22	2.47	0.30

*Indicates the results of the chemical check analysis reported in Table I.

The microprobe data given in Table II also suggest that the apparent solubility of iron in the ELI grade matrix is twice as large as in the normal interstitial alloy. The cause for this effect may be related to lowering the temperature of maximum solubility of iron in the α phase (the eutectoid temperature in the Ti-Fe system)[22] with decreasing amounts of the strong α-stabilizing element oxygen. This conclusion implies that by reducing the interstitial content of Ti-5Al-2.5Sn, the solubility of iron in the α phase is increased. Under equilibrium conditions in alloys with the same iron contents, an increase in the iron solubility would decrease the volume fraction of the iron-rich phase.

The characterization of the microstructures of these alloys using thin foil electron microscopy is in progress and has not been completed. Thin foils of Ti-5Al-2.5Sn were prepared by cutting thin slices about 0.15 mm (0.006 in.) thick parallel to the plate surface with a low speed diamond saw. Discs of the size required for the electron microscope were punched out and hand ground with 600 grit silicon carbide paper to remove burrs. The specimens were electropolished in a jet polishing unit equipped with fiber optics[23] using the electrolyte described by Blackburn and Williams.[24] The temperature of the electrolyte was maintained at -30°C and the operating voltage was 20 volts. The specimens were rinsed in methanol after polishing. The second phase can be observed when the foils are viewed in the light microscope, apparently as a result of differential polishing.[24]

Using this technique, specimens from the air-cooled, normal interstitial material have been observed. The matrix is free of structure with only an occasional dislocation present. Selected area diffraction of the matrix reveal typical hexagonal close-packed diffraction patterns. Long exposure time diffraction patterns have not yet been taken to look for low

intensity α_2 diffraction spots, but the preliminary results indicate no α_2 precipitation has occurred in this alloy.

The second phase observed in the optical microscope has been retained in thin foils. The complicated structure of such a particle from the air-cooled, normal interstitial alloy is shown in Figure 3. Diffraction patterns of these particles are very complex and tilting experiments are currently underway to obtain high symmetry diffraction patterns which are capable of being solved. Using thin foil transmission electron microscopy, Curtis, Boyer, and Williams[10] observed ω precipitation within the β phase in normal interstitial grade Ti-5Al-2.5Sn alloy. Based on the morphology of the structure within the particles and the work of Curtis, et al.,[10] it is believed that the second phase is β with ω formed within it. Hickman[25] has studied the kinetics of ω precipitation in a titanium-7 weight percent iron alloy. Isothermal aging that alloy for one hour at 400°C (752°F) or 450°C (842°F) resulted in 70 percent of the β matrix being transformed to ω as measured using single crystal x-ray techniques. Considering the relatively slow cooling rates of the Ti-5Al-2.5Sn plates under investigation here, it seems likely that ω could form within the second phase (presumably β) with an iron content of 6.5 weight percent.

Another aspect of the microstructure which must be considered when describing α titanium alloys is the crystallographic texture. The overall plate texture and texture gradients were determined by Boeing Technology Service of Seattle, Washington. The pole figures were determined using specimens of the type developed by Leber[26] and the technique of Lopata and Kula.[27] Specimens were cut from the plates so that the normal to the specimen surface made equal angles (54° 44') with the longitudinal (L), transverse (T), and short transverse (S) directions. This geometry has the advantage that the texture will be averaged over the full thickness of the plate and that

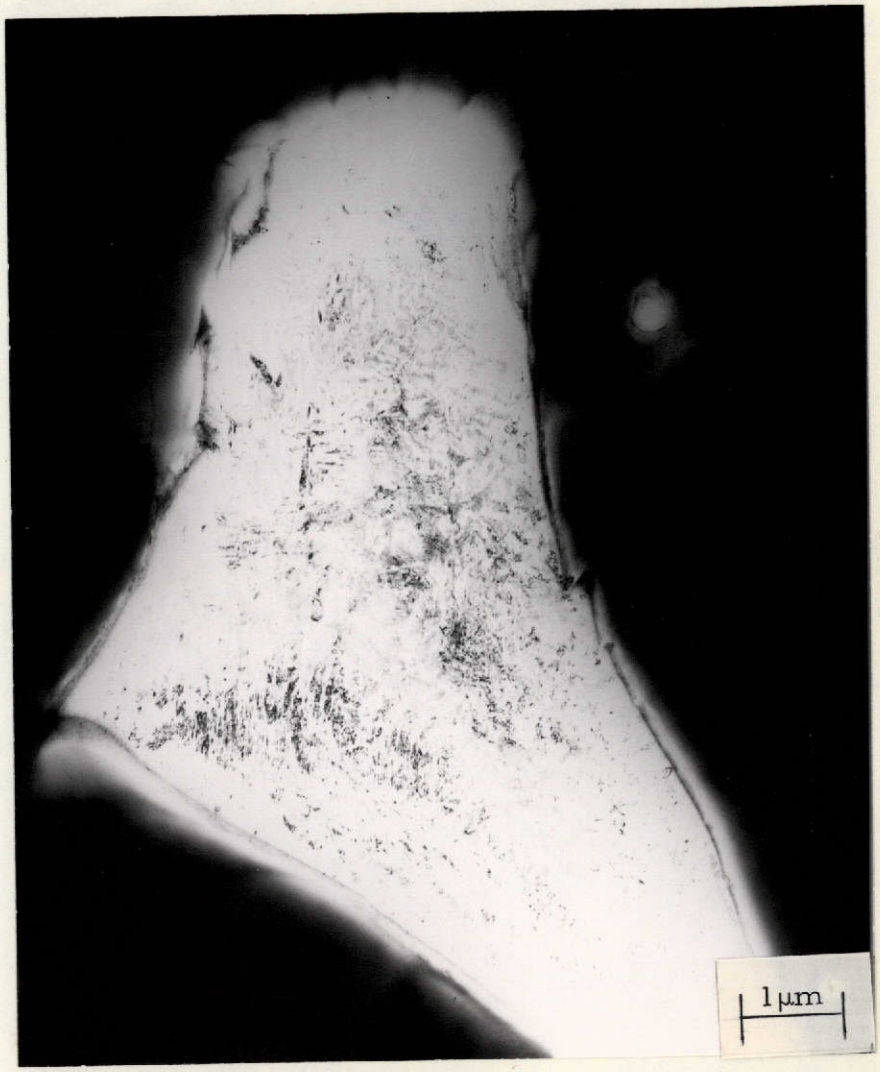

Figure 3. Transmission electron micrograph showing the complex structure of the dispersed phase in the air-cooled, normal interstitial Ti-5Al-2.5Sn alloy.

the texture around all three directions can be determined from a single specimen. Use of a specimen whose normal is parallel to the S direction would give no information about the texture at the L or T poles because texture measurements can only be made 70° away from the specimen normal without major intensity corrections. The pole figures were computer plotted using the techniques and equipment described by Olsen.[28]

In the Ti-5Al-2.5Sn alloys under investigation here, pole figures are to be determined for the basal (0002) prism $(10\bar{1}0)$ planes. To date only the pole figures for the air-cooled, ELI plate have been determined. The pole figures for one quadrant are given in Figure 4 where the notation describing the plate orientations is that used above. The lines shown are the isointensity lines determined by the computer plotting technique[28] and an intensity of one is equivalent to random intensity. The maximum basal texture is twice the random intensity and the basal planes (0002) tend to be parallel to the plate surface. This is a very modest texture when compared to textures in a titanium sheet where intensitities sixty times greater than the random intensity are not unusual.[30, 31] There is a tendency for the basal texture to be split toward the transverse direction and away from the rolling direction. The basal texture reported here is similar to the texture described by Lee and Backofen[32] for annealed normal interstitial Ti-5Al-2.5Sn sheet. The maximum intensity of the prism planes $(10\bar{1}0)$ is 1.5 times the random intensity and occurs around the rolling direction. Ordinarily, one would expect the $(10\bar{1}0)$ pole figures to exhibit six-fold symmetry, but that did not occur in this alloy. The overall texture of this plate can be described as a mild basal texture while the prism planes seem to be perpendicular to the rolling direction.

Olsen and Smith[29] have reported extreme texture gradients in Ti-6Al-4V and developed a color anodization technique to observe these

Ti-5Al-2.5Sn, ELI, AIR-COOLED POLE FIGURES

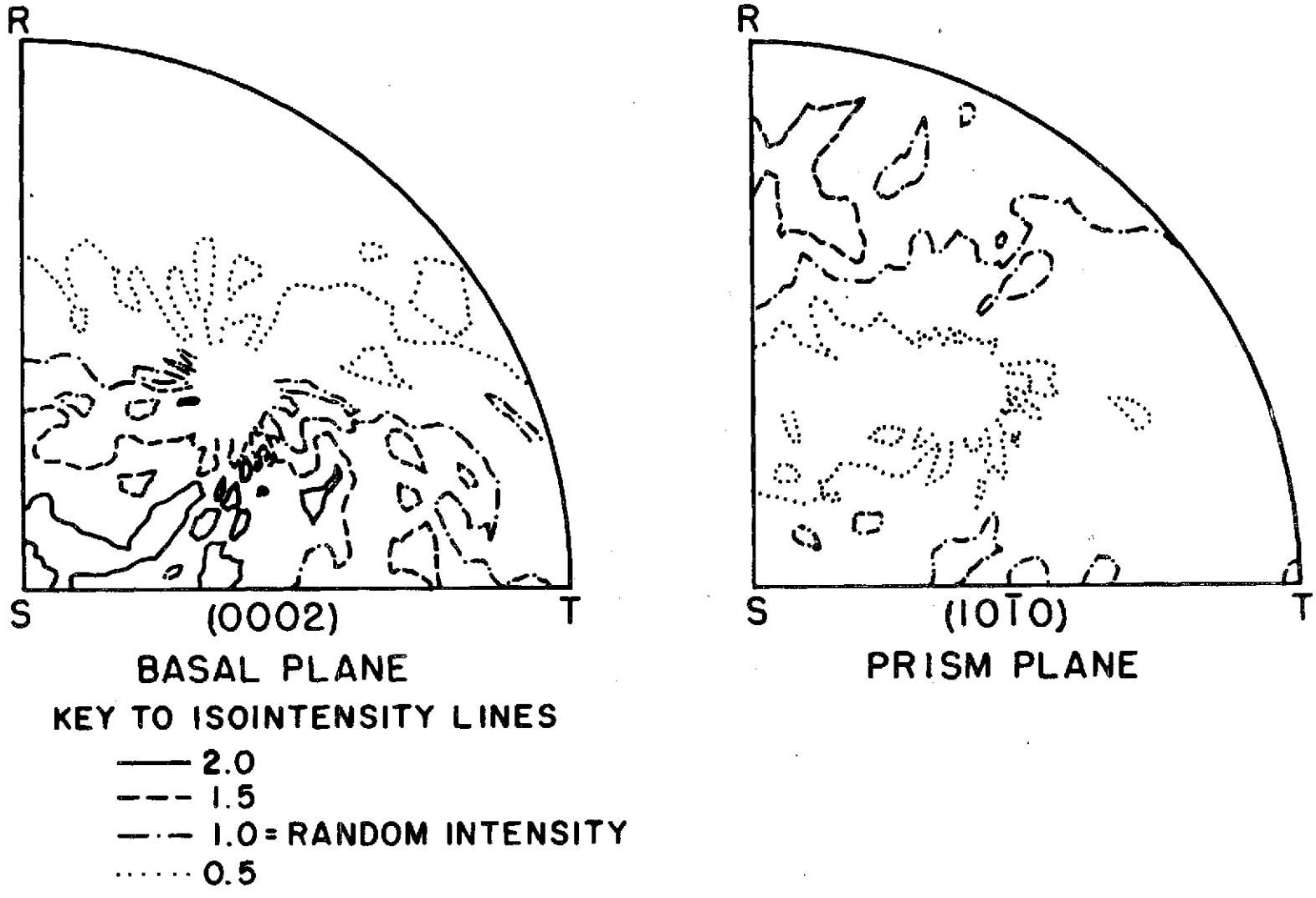

Figure 4. Pole figures of the air-cooled, ELI Ti-5Al-2.5Sn plate.

gradients. Using this method, α grains with basal planes parallel to a metallographic surface are white and as the angle between the c-axis and specimen normal become non-zero, the grains become darker. Thus, from a metallographic specimen, one can get a qualitative picture of texture within a given material.

To determine if a texture gradient occurred in the air-cooled ELI plate, the composite micrograph in Figure 5 was prepared using the color anodization technique of Olsen and Smith.[29] The white bands, or grains with their basal planes parallel to the metallographic surface, are parallel to the rolled surface of the plate. Fewer basal planes seem to be parallel to the plane perpendicular to the rolling direction, which is consistant with the (0002) pole figure in Figure 4. The texture banding is uniform through the plate thickness so that the overall texture described by the pole figures can be considered to be the plate texture. The widths of the bands are much smaller than the dimensions of the mechanical testing specimens, so the results of those specimens should tend to average the effects of the texture banding.

B. Ti-11.5Mo-6Zr-4.5Sn (Beta III)

A 2 cm (0.8 inch) thick plate of Beta III was procured from Colt Industries. It was processed from an ingot to an 11.25 cm (4.5 inch) thick slab by forging, starting at 1093°C (2000°F). Following conditioning, the slab was hot rolled to 2 cm (0.8 inch) thick plate starting at 1121°C (2050°F) and finishing at a low temperature to produce a cold-worked structure. When the resulting microstructure is solution treated, it helps to avoid precipitation of primary α along β grain boundaries. Guernsey, Petersen, and Froes[16] have reported that this type of primary α formation results in strength, fracture toughness, and stress corrosion properties which are lower than in alloys with no primary α present. The plate was then given a sub-β transus solution treatment at 719°C (1325°F) for 15 minutes followed by a water quench The plate was supplied by the producer in the solution treated condition.

Table III shows the composition specification, heat analysis, and check analysis for the Beta III plate. The check analysis was performed by Ti Tech International of Pomona, California. Both the heat analysis and check analysis are within the specification. Comparison of the two analyses indicate there is no large alloy segregation in this material.

The microstructure of the solution treated plate etched with a 30% HNO_3, 2% HF, H_2O solution, as observed in the optical microscope, is shown in Figure 6. In this micrograph, the longitudinal direction is horizontal and the transverse direction is vertical. The darkly etched regions are oriented along the rolling direction and could be observed on polished and etched surfaces with the naked eye. Within the light regions, the outline of equiaxed β grains could be observed, as shown more clearly in Figure 7. This suggests that the dark regions are nonrecrystallized β.

Microhardness tests were performed on the bands using a Vicker's 136° diamond pyramid indentor and a load of 100 grams. Ten measurements were performed in each type of band. Care was taken to assure that the indentations were at least five times the indentation diagonal (~ 25 μm) from a band interface. The average Vicker's pyramid hardness (VPH) of the light bands was 337 with a standard deviation of 13. The dark bands had an average VPH of 351 and a standard deviation of 13. From the results of a t test,[33] it can be concluded that the hardness of the light and dark bands are different at least 95 percent of the time. The fact that the dark bands have a higher hardness than the light bands supports the contention that the dark bands may be nonrecrystallized β.

To show that the etching behavior of the bands did not result from alloy segregation, microanalysis of the bands was performed using a scanning electron microscope (SEM) equipped with an energy dispersive analyzer. The secondary electron image of the region which was studied is shown in

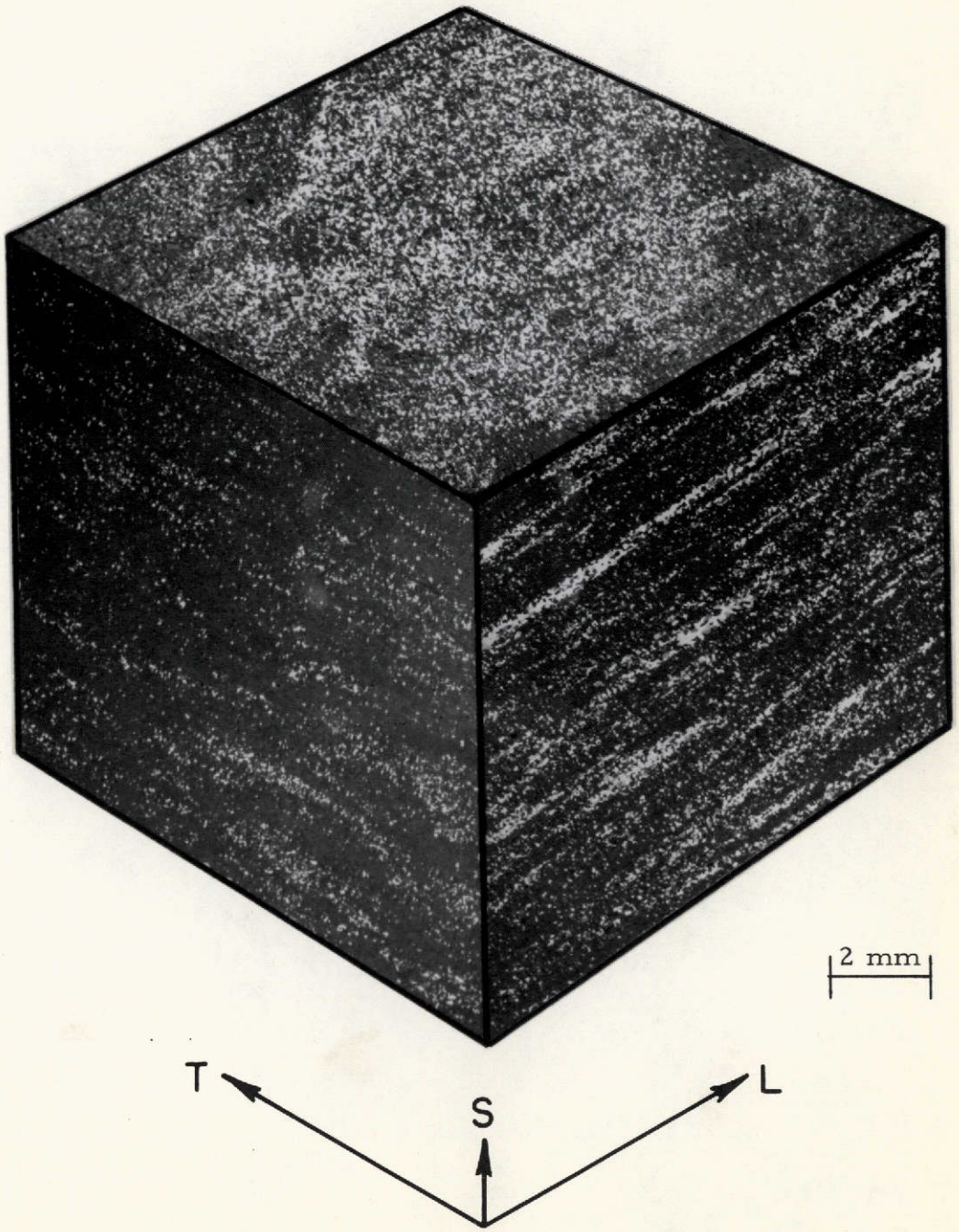

Figure 5. Composite micrograph of color anodized air-cooled, ELI Ti-5Al-2.5Sn alloy. (The surfaces shown are perpendicular to the longitudinal (L), transverse (T), and short transverse (S) directions.)

TABLE III

CHEMICAL ANALYSES OF BETA III (Ti - 11.5 Mo - 6 Zr - 4.5 Sn)
(Weight Percent)

	Mo	Zr	Sn	Fe	O	H	C	N
Specification	10.00/13.00	4.50/7.50	3.75/5.25	0.35 Max	0.18 Max	0.020 Max	0.100 Max	0.050 Max
Heat Analysis	10.2	5.8	4.7	0.03	0.13	0.0143	0.02	0.014
Check Analysis	10.82	5.56	4.60	0.050	0.130	0.0027	0.0104	0.0110
Maximum Error in Check Analysis	0.200	0.100	0.150	0.010	0.0100	0.0010	0.0010	0.0010

Figure 8 where the light spots indicate the spots where the microanalyses were performed. It should be noted that bands which are light in the SEM may or may not correspond to the light bands observed in the optical microscope because the contrast mechanisms in the two instruments are different. The SEM was operated at 25 kv and the detector was run for 100 second accumulations. Because no standards were used and because L_α radiation peaks were present for molybdenum, zirconium, and tin, the values determined were the zirconium-to-molybdenum and tin-to-molybdenum ratios. They were determined by taking the ratios of the maximum L_α intensities corrected only by subtracting the appropriate background intensities. The SEM microanalysis ratios are given in Table IV along with the ratios calculated from the bulk analysis reported in Table III. The values of the ratios from the check analysis, SEM light bands, and SEM dark bands are remarkably similar so that it can be concluded that there is no gross segregation between the light and dark bands. Because of the absence of alloy partitioning, it was not necessary to prove whether the bands which are light in the optical microscope are light or dark in the SEM image.

The objective of the Beta III study is to determine the microstructural features responsible for the large differences in fracture toughness between α-aged and ω-aged plate having similar strength levels. The β+α microstructure was produced by aging at 496°C (925°F) for eight hours followed by air-cooling. This is the treatment suggested by Froes[34] which should result in an improved strength-ductility combination. He also suggested that a slower heating rate improved the toughness; thus the plate was aged in a muffle furnace requiring one hour to reach the aging temperature. Based on the work of Feeney and Blackburn[15] and an isothermal aging study reported in a later section, Beta III was aged at 371°C (700°F) for 3.5 hours and air cooled to create a β+ω microstructure with a strength similar to the α-aged plate.

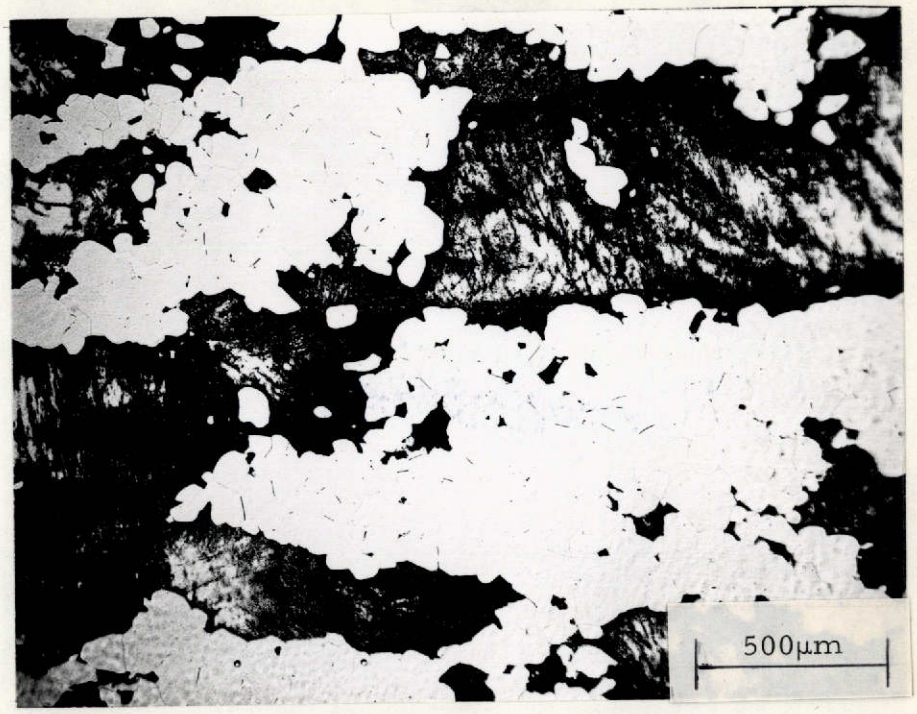

Figure 6. Optical micrograph of solution treated Beta III showing etching bands. (Rolling direction is horizontal and the transverse direction is vertical.)

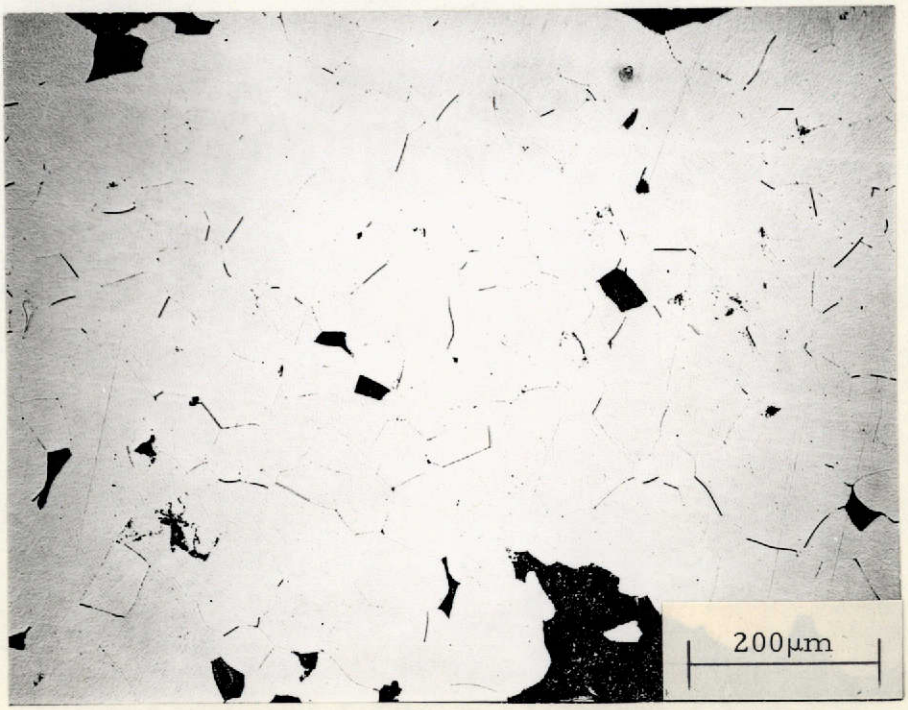

Figure 7. Optical micrograph of solution treated Beta III within a light band. (Rolling direction is horizontal and the transverse direction is vertical.)

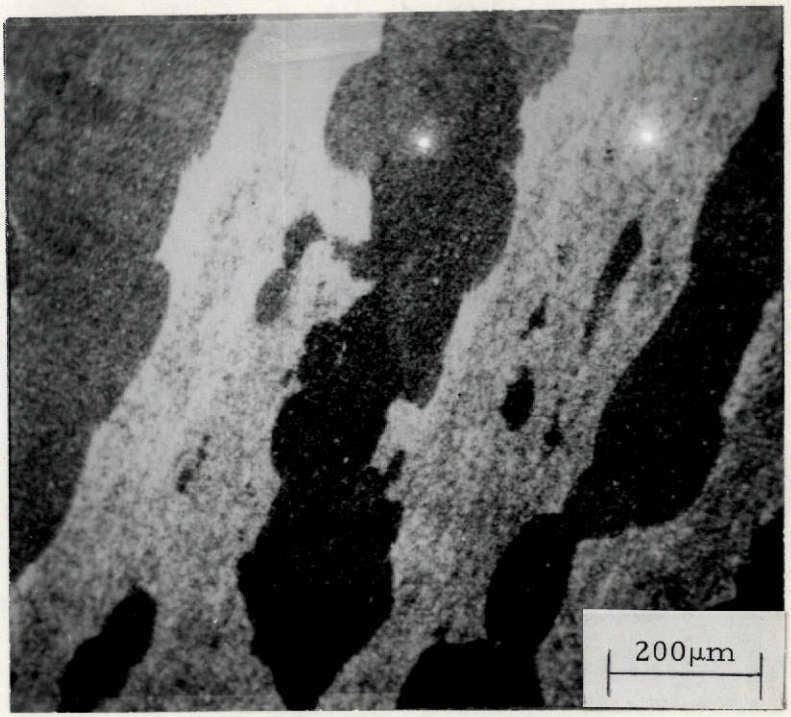

Figure 8. Scanning electron micrograph of solution treated Beta III. (Light spots indicate the regions where the microanalyses were performed.)

TABLE IV

RESULTS OF SEM MICROANALYSES
ON
SOLUTION-TREATED BETA III

Microstructural Feature	Zr/Mo Ratio	Sn/Mo Ratio
SEM Light Band	0.51	0.44
SEM Dark Band	0.48	0.42
Bulk Analysis*	0.51	0.43

*Calculated from check analysis reported in Table III.

No thin foil transmission electron microscopy has been completed on this alloy, but the structure of the α-aged Beta III has been observed using transmission electron microscope replicas from a metallographic specimen etched with a 2% HF-H_2O solution and is shown in Figure 9. Precipitates which are believed to be the α phase seem to have two different size distributions. The larger ones are 1 to 2 μm in length and about 0.25 μm wide and seem to align themselves as if they precipitate on a structural boundary. This suggests that they are primary α which form on a β grain boundaries. The smaller α-aging precipitates are about 0.25 μm in size and seem to have precipitates homogeneously in the β matrix.

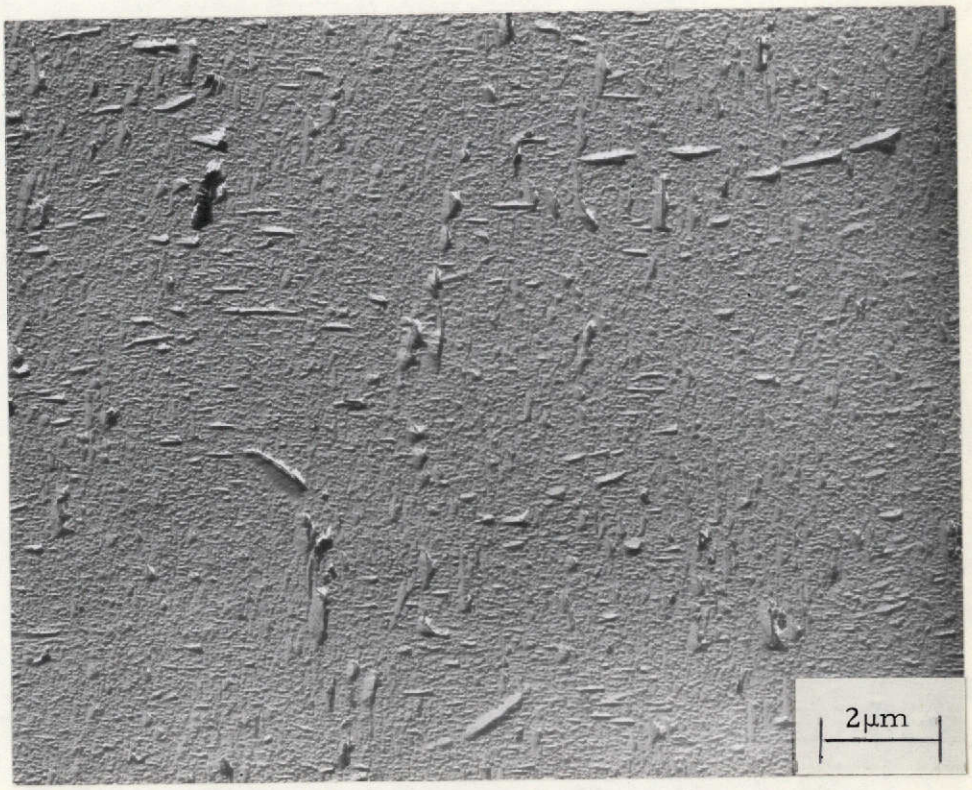

Figure 9. Transmission electron replica micrograph showing structure of α-aged Beta III.

MECHANICAL PROPERTIES

During this investigation tensile tests, compression tests, and plane strain fracture toughness (K_{Ic}) tests were performed. All three types of tests were conducted at room temperature (295°K or 72°F) but only tensile and K_{Ic} tests were performed at the temperatures of liquid nitrogen and liquid hydrogen--77°K (-320°F) and 20°K (-423°F), respectively. Before the results of these tests are presented, the techniques used will be described.

For the Beta III study, it was intended to match the tensile yield strengths of the $\beta+\alpha$ and $\beta+\omega$ aged structures. However, the ω-aged material was so brittle that conventional tensile specimens failed before macroscopic yielding. It therefore became necessary to match strength levels for the two structures on the basis of their compressive yield strengths. Compression tests were initially performed using an Instron compression load cell and an Instron extensometer on a cylindrical test specimen with a nominal diameter of 0.5 cm (0.2 inch) and a length-to-diameter ratio of five. One of the first specimens tested in this fashion buckled, resulting in the destruction of the extensometer. To avoid that situation in the future, the specimen length-to-diameter ratio was reduced to four and the compressive stress-strain curve was determined by subtracting the effect of the testing apparatus compliance from the load-time test record.

The load cell and the moving platen were aligned to within 0.0025 mm (0.0001 inch) of being parallel. The compliance of the testing system was determined by placing a hardened steel block with a cross-sectional area larger than the platens between the two parallel surfaces. At a crosshead speed of 0.025 cm/min (0.010 inch/min.), the load-time curve was monitored. As is typical with Instron equipment, the machine deflection

(crosshead speed x time) did not vary linearly with the load, so the deflection-load data were fitted by a least squares method to a fifth order polynomial expression.

The compression tests were run with both platens lubricated with teflon. About one hundred data points from each load-time plot were read into a computer program which subtracted the deflection of the machine as calculated with the polynomial expression from the total deflection monitored during the test. The loads and specimen dimensions were used to calculate points along the engineering stress-strain curve. The initial linear slope was constructed and the 0.2% offset compression yield stress was determined.

The tensile and fracture toughness properties at 295° (72°F) and 77°K (-320°F) were determined at Carnegie-Mellon University while the properties at 20°K (-423°F) were determined at the NASA Lewis Research Center. The 77°K tests were performed in a foam insulated, stainless steel dewar filled with liquid nitrogen which was part of the load train of a 27,000 kg (60,000 lb.) universal testing machine. The 20°K tests were performed in a vacuum insulated, liquid hydrogen cryostat built within a 550,000 kg (1.2 million pound) universal testing machine. The construction, safety features, and capabilities of the liquid hydrogen testing facility have been described by Shannon.[35] The specimens and techniques used in each facility are different and will be described separately.

At the higher temperatures (295°K and 77°K), the tensile specimens were cylindrical samples with a nominal diameter of 6.25 mm (0.25 inch). A linear variable differential transformer (LVDT) extensometer with a 2.54 cm (1 inch) gage length and capable of a 15 percent extension was used to record the specimen extension up to the point of maximum load. The output gain and phase angle between the primary and secondary signals of the LVDT

were adjusted in a way that the calibration at room temperature and liquid nitrogen temperature were the same. This technique was developed by Shannon[36] and described previously.[1] In this way, a careful room temperature calibration applied equally well at liquid nitrogen temperature. Load and extension were autographically recorded up to the maximum load. Beyond the maximum load, the minimum diameter was measured with a point micrometer and the corresponding load was recorded periodically up to fracture. For tests conducted in liquid nitrogen, the specimens were strained in the liquid nitrogen cryostat, removed, and allowed to warm to room temperature, the minimum diameter was measured, and the specimens were cooled to 77°K before they were strained again.

The fracture strain was calculated from the minimum diameter of the fractured specimen. The measure of strain used throughout this report is the diametral strain (ϵ) which is defined in Equation (1).

$$\epsilon = 2 \ln (d_o/d) \tag{1}$$

where

d_o = initial specimen diameter

and d = instantaneous specimen diameter.

The load-extensometer trace was used to determine the 0.2% offset yield strength (σ_y) and the ultimate tensile strength (UTS).

The load-extension trace and the data taken after the point of maximum load was used to determine a true stress-plastic strain curve using the standard corrections.[37] The true stress data was corrected using the Bridgman correction[38] to account for the component of balanced triaxial stress state which exists in the necked region of a tensile specimen. The flow stress (σ) is calculated by multiplying the true stress by the Bridgman correction factor (F) for cylindrical specimens, which is given in Equation (2).

$$F = 1/\{ (1+2R/a) \ln (1+a/2R) \} \quad (2)$$

where

a = minimum radius of the necked region

and R = radius of curvature of the neck.

This factor is a function only of the a/R ratio of the necked region. Previous work[1] on Ti-5Al-2.5Sn alloys tested at room temperature has shown that a/R can be related linearly to the plastic strain (ε) by the following equation

$$a/R = -0.072 + 0.589\ \varepsilon \quad (3)$$

According to this relationship, a/R would be negative below strains of 0.12. This is the region of uniform plastic strain where no neck has developed so the true stress is considered to be the flow stress. Above strains of 0.12, Equations (2) and (3) are used to calculate the Bridgman correction factor and the flow stress.

A computer program has been written to calculate the plastic strain, true stress, and flow stress for each datum point from the load, extension, and minimum diameter data. Empirical flow curves are then determined by relating the flow stress (σ) to the plastic strain (ε) using Equation (4)

$$\sigma = \sigma_o + A\varepsilon^m \quad (4)$$

where

σ_o, A, and m = constants determined by a least squares regression technique.

Monteiro and Reed-Hill[39] have shown that this form of a flow curve fits the experimental data of titanium better than the more traditional form where σ_o equals zero. This is also true for the alloys studied in this investigation.

The plane strain fracture toughness tests performed at 295°K and 77°K used standard compact tension specimens[40] 1.88 cm (0.75 inch) thick

for Beta III and 2.5 cm (1 inch) thick for Ti-5Al-2.5Sn. The displacement at the mouth of the machined notch was measured with a spring-loaded LVDT clip gage seated in knife edges attached to the specimen. Figure 10 shows the LVDT clip gage attached to a 2.5 cm (1 inch) thick compact tension specimen. This clip gage is similar to the one designed by Shannon.[35, 36] It was calibrated so that the calibrations at 295°K and 77°K were identical using the technique developed by Shannon[36] which was described previously.[1] All the features of this test facility met the ASTM requirements for plane-strain fracture toughness testing.[40]

The liquid hydrogen (20°K) tensile tests were performed on cylindrical specimens with a nominal diameter of 1.8 cm (0.45 inch). Strain was measured using two foil resistance strain gages mounted on the central portion of the specimen gage length 180° apart. Load and strain were recorded on an X-Y-Y' recorder with the output of each strain gage fed to a separate pen. The strain gages usually failed shortly after the 0.2% offset strain was reached. The test record was used for the determination of Young's modulus and the 0.2% offset yield stress. No load-time record was maintained during the remainder of the test but the maximum load and the load at which the specimen ruptured was read from the load dial on the testing machine. The information from the load-extension curve, the fracture load, and the minimum diameter of the fractured specimen were used in the computer program previously described to determine the constants of the empirical flow curve equation given in Equation (4).

Two sizes of three-point bend plane-strain fracture toughness specimens[40] were used to determine K_{Ic} in liquid hydrogen: 2.5 cm (1 inch) in thickness by either 2.5 cm (1 inch) or 5 cm (2 inchs) in width (referred to as 1x1 and 1x2 bend specimens, respectively, throughout the balance of this report). Both of these specimen designs are recommended in the ASTM

test method.[40] The displacement at the mouth of the machined notch was measured with a strain-gaged double cantilever clip-in displacement gage[40] attached to integrally machined knife edges. The strain gage excitation voltage was 1.5 volts and the output signal was amplified 10 times before it was fed into an X-Y recorder. With this low excitation voltage, no boiling of liquid hydrogen occurred at the clip gage arms and extraordinarily clean test records were obtained. This test facility met all the requirements set by the ASTM standard K_{Ic} test method.[40]

To date, 58 fracture toughness tests have been conducted. Nine of these tests are considered invalid based on the ASTM criteria for fatigue crack front straightness.[40] According to the ASTM test method,[40] the crack length at the center of the specimen and at the positions halfway between the center and edge of the specimens may not deviate from the average of these three lengths by more than 5 percent. If the deviation exceeds 5 percent, the test result is considered invalid. This is an arbitrary requirement,[41] so an analysis of the test results was performed to find if this requirement could be relaxed from 5 to 10 percent. If this were done, only one test would fail to qualify on the basis of crack front straightness.

To determine if the acceptable crack front deviation could be relaxed to 10 percent, a statistical analysis was performed to examine the influence of crack front straightness on the measured K_Q (conditional value of K_{Ic}). To avoid confusion with respect to specimen geometry and the alloys being investigated, the correlations were run on three groups--Ti-5Al-2.5Sn alloys tested using compact tension specimens, Ti-5Al-2.5Sn alloys tested using bend specimens, and α-aged Beta III specimens. The only data used in the correlation were test results which were totally valid or results which were invalid only because the crack front deviation exceeded 5 percent. The single specimen whose crack front straightness deviation exceeded 10 percent

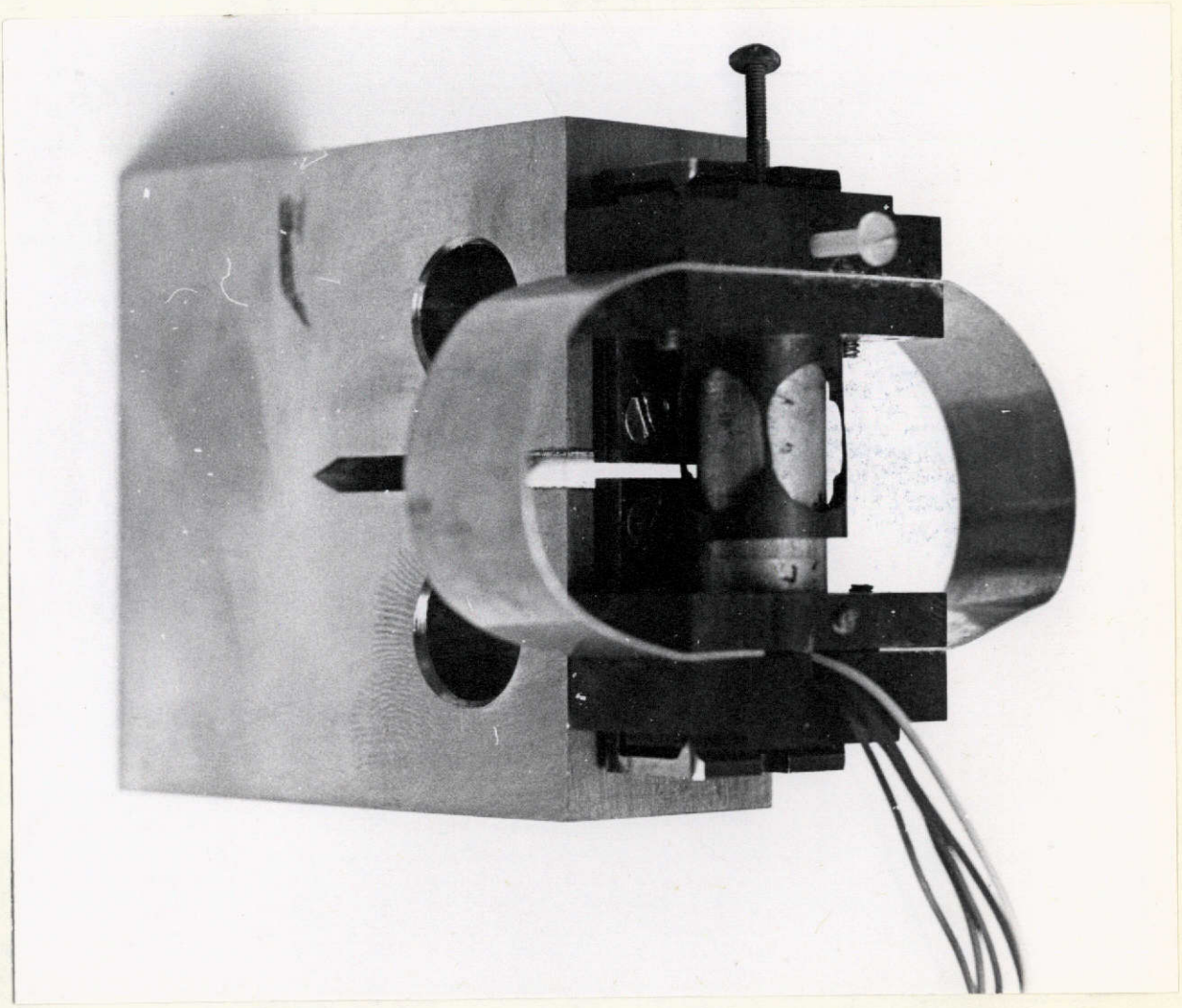

Figure 10. Photograph of LVDT clip gage mounted on a 2.5 cm (1 inch) thick compact tension K_{Ic} specimen.

was not considered. It is interesting to note that this was the only specimen whose crack length at the edge of the specimen exceeded those at the three central positions. The fracture toughness data of each set (each having common composition, heat treatment, specimen orientation, and test temperature) were normalized by dividing the individual test results by the average of the totally valid K_{Ic} results of that set. A linear least squares regression was performed on the normalized fracture toughness data as a function of crack front straightness deviation. The slope of the resulting line was compared using a t test[42] with a slope of zero, a condition of no effect of deviation on K_{Ic} to determine the probability that the two values are different. The resulting data are shown in Table V. The sign of the correlation coefficient indicates the way in which the normalized fracture toughness varied with increasing deviation. The correlation coefficient and significance for the two Ti-5Al-2.5Sn sets are low and can be concluded that the effect of crack front straightness deviation on K_{Ic} is doubtful. Based on the results of four specimens of α-aged Beta III, there seems to be a real effect of crack front deviation on K_{Ic}, but before such a statement is confirmed, more data on Beta III must be analyzed.

As a result of the above correlation analysis, Ti-5Al-2.5Sn K_{Ic} data reported as valid data will include results from specimens with crack front deviations up to 10 percent, but the crack front straightness criterion used on Beta III was held at 5 percent.

A study of the effect of crack front straightness on K_{Ic} in aluminum alloys using techniques similar to those described above concluded that the acceptable deviation could be relaxed to 10 percent without adversely affecting the ability to measure K_{Ic}.[41] As a result of these studies, there is evidence that the 5 percent crack front straightness criterion may be too restrictive. A conscious effort should be made to statistically analyze K_{Ic}

TABLE V

RESULTS OF THE STATISTICAL ANALYSIS OF THE EFFECT OF FATIGUE CRACK FRONT STRAIGHTNESS ON K_{Ic}

Alloy/Specimen Group	Number of Specimens	Correlation Coefficient	Statistical Significance
Ti-5Al-2.5Sn Compact Tension Specimens	15	-0.264	68%
Ti-5Al-2.5Sn Bend Specimens	32	0.171	66%
α-Aged Beta III Compact Tension Specimens	4	-0.979	98%

results from a wide range of materials in order to experimentally determine the effect of crack front straightness on K_{Ic} and possibly revise the current recommended Test Method.

A. Ti-5Al-2.5Sn

The mechanical properties of the Ti-2Al-2.5Sn alloys were determined at 295°K (72°F), 77°K (-320°F), and 20°K (-423°F). The conventional tensile properties were determined in the longitudinal direction. The plane strain fracture toughness at 295°K and 77°K was determined from 2.5 cm (1 inch) thick compact tension specimens in the LT orientation (crack plane perpendicular to the plate longitudinal direction and crack propagation in the transverse direction). At 20°K, the plane strain fracture toughness was determined for the LT and LS (crack plane perpendicular to the longitudinal direction and crack propagation in the short transverse direction) orientations using three point bend specimens of two sizes: 1x1 and 1x2 specimens for the LT orientation, 1x1 specimens for the LS orientation. Thus, the applied load in all the specimens acts parallel to the longitudinal direction. The one-inch width of the LS orientation specimens was limited by the plate thickness. They were included for comparison with surface crack specimen results being obtained at NASA Lewis Research Center using the same experimental material. The two specimen sizes tested in the LT orientation were intended to explore possible specimen size effects and thereby qualify the results from the 1x1 specimens tested in the LS orientation for comparison with the 1x1 specimens tested in the LT orientation for the purpose of identifying toughness directionality in the plate product.

The tensile and fracture toughness properties of the Ti-5Al-2.5Sn alloys are given in Table VI. These data represent the averages and standard deviations of multiple tests except where otherwise noted. The specimen

TABLE VI

MECHANICAL PROPERTIES OF TITANIUM ALLOYS

(Data indicates the mean ± one standard deviation)

Alloy	Test Temperature °K (°F)	σ_y 0.2% Yield Strength (ksi) (a)	Ultimate Tensile Strength (ksi) (a)	Tensile Fracture Strain	K_{Ic} (ksi/in.) (b)	K_{Ic} Specimen Orientation (f) and Type
Ti-5Al-2.5Sn	295 (72)	102.1 ± 0.8	110.2 ± 1.1	0.528 ± 0.012	107.9 (c, d, g)	LT-CT (e)
ELI	77 (-320)	171.4 ± 2.0	181.9 ± 0.6	0.407 ± 0.041	101.1 ± 4.4	LT-CT
Air-Cooled	20 (-423)	189.0 ± 1.0	203.5 ± 0.8	0.254 ± 0.028	81.5 ± 4.5	LT-1x2 Bend
					82.7 ± 1.8	LT-1x1 Bend
					96.9 ± 4.5(g)	LS-1x1 Bend
Ti-5Al-2.5Sn	295 (72)	98.9 ± 0.7	108.4 ± 0.4	0.512 ± 0.025	104.9 (c, g)	LT-CT
ELI	77 (-320)	170.6 ± 0.5	180.5 ± 1.0	0.402 ± 0.024	75.1 ± 0.4	LT-CT
Furnace-Cooled	20 (-423)	189.4 ± 0.3	204.7 ± 1.6	0.207 ± 0.043	64.0 ± 1.1	LT-1x2 Bend
					61.8 ± 2.2	LT-1x1 Bend
					73.4 ± 5.1	LS-1x1 Bend
Ti-5Al-2.5Sn	295 (72)	126.9 ± 0.5	133.8 ± 0.4	0.435 ± 0.040	65.4 ± 4.4	LT-CT
Normal Interstitial	77 (-320)	194.5 ± 1.0	207.3 ± 1.1	0.317 ± 0.015	48.6 ± 1.3	LT-CT
Air-Cooled	20 (-423)	215.4 ± 2.3	228.9 ± 0.1	0.209 ± 0.029	46.8 ± 1.0	LT-1x2 Bend
					46.0 ± 1.0	LT-1x1 Bend
					45.7 ± 0.4	LS-1x1 Bend
Ti-5Al-2.5Sn	295 (72)	127.9 ± 0.6	132.6 ± 0.6	0.328 ± 0.055	60.0 ± 1.3	LT-CT
Normal Interstitial	77 (-320)	200.0 ± 0.5	209.9 ± 0.3	0.327 ± 0.034	52.5 ± 1.8	LT-CT
Furnace-Cooled	20 (-423)	220.3 ± 1.2	228.7 ± 0.4	0.124 ± 0.051	46.2 ± 0.2	LT-1x2 Bend
					42.7 ± 0.3	LT-1x1 Bend
					47.8 ± 3.3	LS-1x1 Bend
α-Aged Beta III	295 (72)	185.7 ± 1.8	196.6 ± 0.6	0.102 ± 0.009	49.8 ± 1.2	LT-CT
(496°C/8 hours)	295 (72)	180.5 ± 2.9	compression test			
ω-Aged Beta III	295 (72)					LT-CT
(371°C/3.5 hours)	295 (72)	187.2 ± 1.4	compression test			

(a) 1 ksi = 6.9 MN/m^2

(b) 1 ksi/in = 1.1 $MN/m^{3/2}$

(c) This result is invalid because specimen thickness is less than 2.5 $(K_{Ic}/\sigma_y)^2$. Only one test was conducted.

(d) This result is invalid because the maximum load exceeded the 5% tangent load by more than 10%.

(e) CT indicates a compact tension specimen.

(f) Orientation notation is that of ASTM E399-74.

(g) This result is invalid because crack length is less than 2.5 $(K_{Ic}/\sigma_y)^2$.

measurements and other results of the individual fracture toughness tests are given in Appendix A.

Figure 11 shows the longitudinal strength and LT orientation fracture toughness data for Ti-5Al-2.5Sn plates as a function of testing temperature. The error bars indicate the range of plus and minus one standard deviation (68 percent confidence limits). If no error bar is shown, the standard deviation is smaller than the point representing the average value. The room temperature K_{Ic} tests on the extra low interstitial (ELI) alloys are invalid and represent the results of a single test.

The strength levels of the normal interestitial alloys are about 175 MN/m^2 (25 ksi) higher than the ELI alloys. For both grades, the yield strength at liquid hydrogen temperature is approximately twice that at room temperature. In most cases, the ultimate tensile strength (UTS) is about 70 MN/m^2 (10 ksi) higher than the yield strength. Both the yield strength and ultimate tensile strength seem to decrease linearly with increasing testing temperature, with the exception of the UTS data for the ELI alloys. A paired t test[33] was performed to observe if the cooling rate significantly affected the yield strength. The probability that the yield strengths are independent of cooling rate is 31 percent, which is too low to say that the cooling rate affects the strength level.

The ELI alloys are much tougher than those of the normal interstitial alloys. Increased cooling rate from the annealing temperature has no effect on the toughness of the lower purity alloys, but improves the toughness of the ELI plates by about 30 percent. It is interesting to note that the fracture toughness of the ELI alloys at 20°K is greater than the K_{Ic} of the normal interstitial alloys at room temperature.

Both the air-cooled and furnace-cooled ELI plates have room temperature K_Q results (a conditional value of K_{Ic}) which are invalid because of

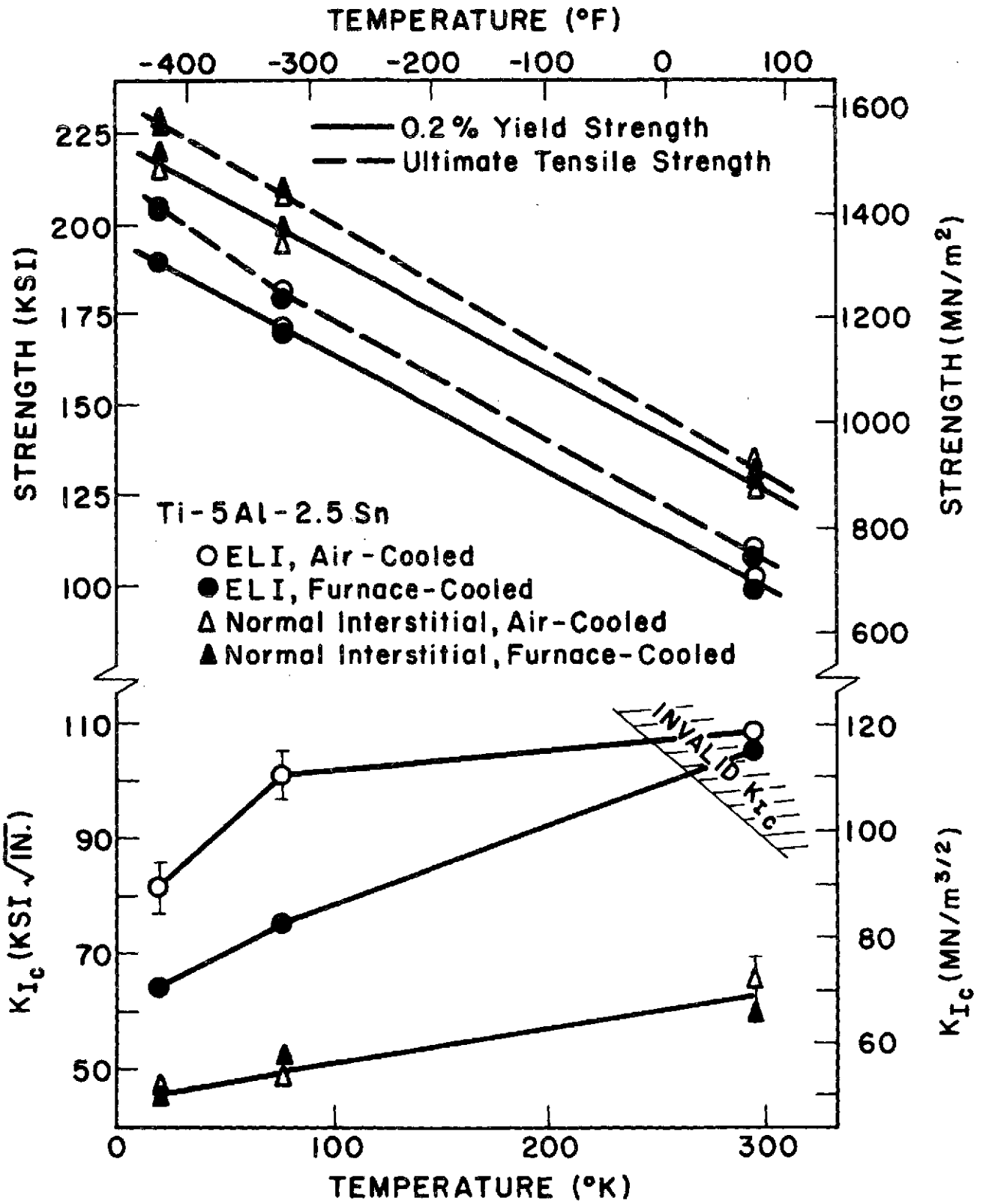

Figure 11. The effect of testing temperature on the longitudinal tensile properties and LT fracture toughness of Ti-5Al-2.5Sn. The error bars indicate the range plus and minus one standard deviation.

insufficient crack length and specimen thickness. In the furnace-cooled specimen, the maximum load and fast fracture occurred at specimen deflections less than the 5 percent secant deflection. In the air-cooled specimen, however, the maximum load exceeded the 5 percent secant load by 32 percent and fast fracture occurred at a specimen deflection much greater than that of the 5 percent secant. This test was considered invalid because a specimen whose maximum load exceeds the 5 percent secant load by more than 10 percent would fail to meet the requirements of the ASTM Test Method.[40] These observations of the test records suggest that at room temperature the air-cooled ELI plate may be tougher than the furnace-cooled ELI plate even though these materials have similar K_Q values.

It is interesting to compare the properties of the Ti-5Al-2.5Sn alloys to other alloys which are used to store cryogenic liquids. The Al-Mg-Mn alloy 5083-0 is being used in the construction of storage tanks for use in liquified natural gas tankers. Kaufman, Nelson, and Wygonik[43] have measured the properties of thick plate from room temperature to 77°K and shown its yield strength of about 138 MN/m^2 (20 ksi) is relatively independent of temperature. Because of its low strength, a valid K_{Ic} could not be determined, but a conservative estimate for K_{Ic} at 77°K is 66 $MN/m^{3/2}$ (60 ksi$\sqrt{in}$). The toughness at lower temperatures may be slightly higher than that value. When these values are compared to the data on the Ti-5Al-2.5Sn alloys shown in Figure 11, one notes that the air-cooled ELI α titanium alloy is much tougher and almost an order of magnitude stronger than this aluminum alloy at 77°K.

Because alloys usually show trends of decreasing K_{Ic} with increasing yield strength, the toughness of different alloys must be compared at similar strength levels. The fracture toughness of the Ti-5Al-2.5Sn alloys has been plotted as a function of the yield strength in Figure 12. The changes in

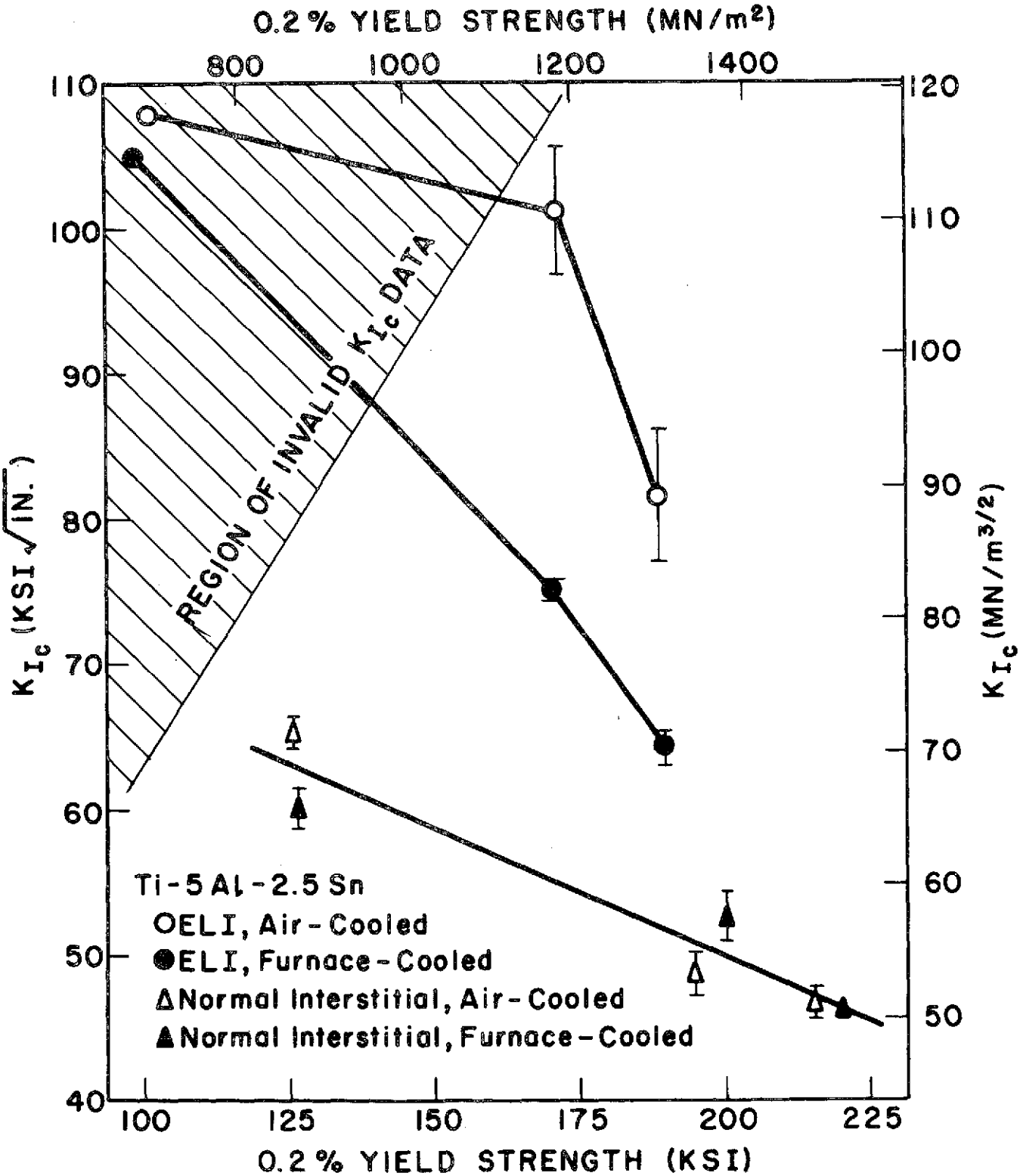

Figure 12. The variation in LT fracture toughness with the longitudinal tensile yield strength of Ti-5Al-2.5Sn. The variations in strength result from changes in testing temperature. The error bars indicate the range plus and minus one standard deviation.

these properties are a result of the testing temperature. The data presented in Figure 12 are the same as that shown in Figure 11 and the error bars have the same meaning as those in Figure 11. The region of invalid K_{Ic} data in Figure 12 is where the specimen thickness and the crack length are too small to meet the ASTM test requirement.[40] The same trends as those noted earlier are observed. At similar strength levels, the ELI alloys are tougher than the normal interstitial alloys. Cooling rate does not seem to greatly affect the K_{Ic} of the normal interstitial alloys, but furnace cooling greatly reduces the toughness of ELI alloys with respect to the K_{Ic} of the air-cooled material. It is interesting to note that these are the same trends that were observed by Shannon and Brown[12] using sharply notched specimens of Ti-5Al-2.5Sn sheet, especially in the thicker specimens.

The results of the three types of bend specimens used to measure K_{Ic} at 20°K (-423°F) are shown in the form of a bar graph in Figure 13. A schematic of the specimen orientations is shown in the inset of the figure. The darkened regions represent the range of K_{Ic} within plus and minus one standard deviation of the mean (68 percent confidence limits). All the K_{Ic} results are valid except those determined from the LS 1x1 bend specimens taken from the air-cooled, ELI Ti-5Al-2.5Sn plate, where the crack lengths were about 15 percent less than the $2.5\,(K_{Ic}/\sigma_y)^2$ length required by the standard Test Method.[40] Statistical t tests[33] were performed to make comparisons between the two sizes of LT orientation specimens and the orientation of the 1x1 bend specimens. When t test results indicate the probability that the two results being compared are different by more than 90 percent, the differences are considered to be a real effect. A comparison between the 1x1 and 1x2 LT bend specimens indicates the K_{Ic} results are the same except for the furnace-cooled, normal interstitial alloy. A comparison between the 1x1 LT and 1x1 LS results indicate there is a significant difference in K_{Ic} with

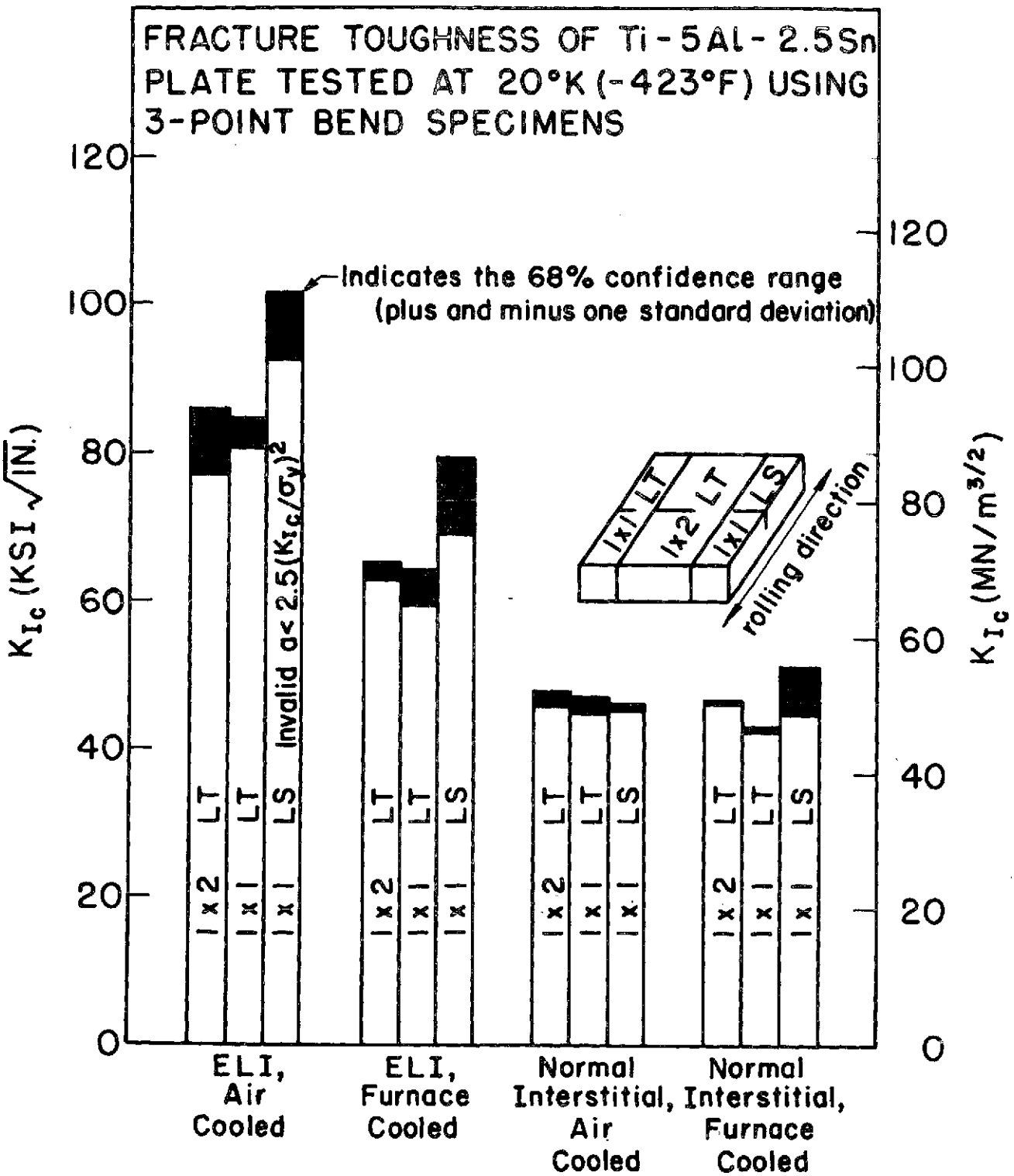

Figure 13. Fracture toughness of the Ti-5Al-2.5Sn plates at 20°K (-423°F) determined using 3-point bend specimens.

specimen orientation except for the air-cooled normal interstitial alloy. In three cases where the orientation effect was observed, the LS specimens have the greatest K_{Ic}.

If the specimen geometry (1x1 versus 1x2 bend specimens) does not affect the ability to measure K_{Ic} as the statistical analysis suggests, the 1x1 LT fracture toughness measurements on the furnace-cooled, normal interstitial alloys seem to be low. The actual difference in K_{Ic} is only 3.0 $MN/m^{3/2}$ (3.5 ksi$\sqrt{in}$) and the reason for the difference being significant is the extremely low standard deviations. If the toughness of these 1x1 LT specimens are low, the liquid hydrogen K_{Ic} results indicate the LS toughness is greater than the LT toughness in the ELI plates but there is no orientation effect in the normal interstitial plates. It is believed that this description of an orientation effect in ELI alloys and an absence of one in the lower purity material is accurate and truly represents the behavior in these alloys.

The tensile flow curves of the Ti-5Al-2.5Sn alloys are shown in Figure 14. The circles shown are experimental data points from multiple specimens and the solid curve is the result of the least squares regression empirical flow curves of the form previously given in Equation (4). The empirical flow curves are terminated at the average fracture strain which is indicated by an "X". Many datum points determined from the load-deflection test record are not shown in Figure 14 but were used in regression analysis. This is the region up to strains of about 0.1 for the 295°K and 77°K flow curves but only up to about 0.01 for the 20°K flow curves. The constants σ_o, A, and m from empirical flow curves are listed in Table VII. The statistical significance, which is also given in Table VII, was calculated using a paired t test[33] by comparing the experimental flow stress with that calculated from the empirical flow curve at the given plastic strain. The significance can be interpreted as the probability that the experimental flow

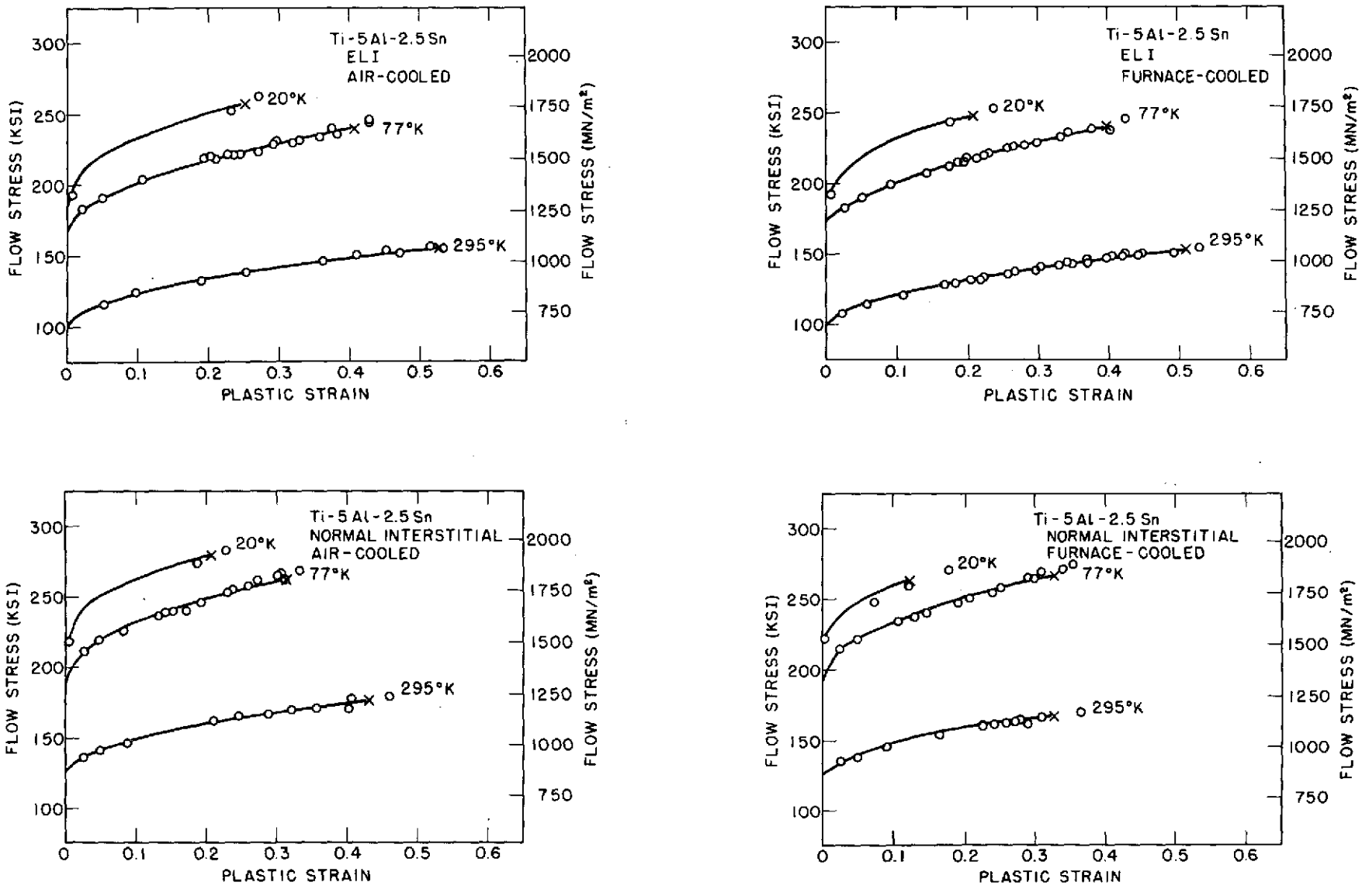

Figure 14. Tensile flow curves of Ti-5Al-2.5Sn. The solid lines are the result of the regression analysis and "X" represents the average fracture strain.

TABLE VII

FLOW CURVES OF TITANIUM ALLOYS FIT TO THE FORM $\sigma = \sigma_0 + A\varepsilon^m$

WHERE σ IS THE FLOW STRESS AND ε IS TRUE PLASTIC STRAIN

Alloy	Test Temperature $^{\circ}K$ ($^{\circ}F$)	σ_0 (ksi) (a)	A (ksi) (a)	m	Level of Significance (%) (b)
Ti-5Al-2.5Sn	295 (72)	98.0	77.5	0.50	93.7
ELI	77 (-320)	166.3	115.8	0.52	98.3
Air-Cooled	20 (-423)	172.5	135.6	0.35	98.8
Ti-5Al-2.5Sn	295 (72)	96.4	81.5	0.54	93.0
ELI	77 (-320)	165.9	121.3	0.55	>99.9
Furnace-Cooled	20 (-423)	171.2	132.4	0.35	97.1
Ti-5Al-2.5Sn	295 (72)	120.5	82.9	0.47	96.8
Normal Interstitial	77 (-320)	180.3	129.2	0.40	96.4
Air-Cooled	20 (-423)	185.8	140.1	0.26	94.7
Ti-5Al-2.5Sn	295 (72)	123.4	81.2	0.55	92.9
Normal Interstitial	77 (-320)	189.9	127.5	0.46	93.2
Furnace-Cooled	20 (-423)	185.8	116.7	0.21	97.2
α-Aged Beta III ($496^{\circ}C$/8 hours)	295 (72)	150.6	96.3	0.17	94.8

(a) 1 ksi = 6.9 MN/m^2

(b) Determined using a **t** - test on paired data.

curve data and the empirical flow curve belong to the same population. The fit of the data is excellent.

Caution must be observed when interpreting the 20°K flow curves because no data was obtained between strains of about 0.01 and the fracture strains which are all greater than 0.1. The tensile tests at 20°K also exhibited a serrated yielding behavior where the stress-strain curve has sudden load drops. Upon further crosshead motion, the load slowly increases to a level above the previous maximum load and then drops suddenly again. This behavior is observed many times during the test of a single specimen. In titanium, this type of behavior has been associated with adiabatic heating effects and mechanical twinning.[44] In the Ti-5Al-2.5Sn alloys investigated here, the maximum load in the specimens tested at 20°K occurs at the fracture load. These specimens also exhibit multiple necking[44] where several necked regions can be observed away from the fracture surface of broken tensile specimens. The serrated yielding and multiple necking behavior were not observed in specimens tested at room temperature or in liquid nitrogen.

Care must be observed when making comparisons between the σ_o values in Table VII because the load extension curves at liquid hydrogen were determined using a testing system which had a strain resolution of 0.00002 while at the higher test temperatures, the recording system had a strain resolution of 0.0001. At these temperatures, the LVDT resolution was purposely reduced so that load-deflection curve up to maximum load could be monitored. The higher strain resolution at 20°K will increase the ability to observe small deviations from linear elastic behavior and thus decrease the apparent elastic limit (σ_o).

The rate of strain hardening as calculated from the empirical flow curve ($\partial\sigma/\partial\varepsilon = mA\varepsilon^{m-1}$) is greater at 77°K than at room temperature. The

strain hardening behavior is independent of alloy purity and cooling rate and seems to be only a function of testing temperature. The strain hardening at the liquid hydrogen temperature seems to be similar to that of the temperature of liquid nitrogen, but this result is questionable because of the uncertainty of the 20°K flow curves. The difference in the flow curves between the ELI and normal interstitial alloys result largely from the apparent elastic limit (σ_o) increasing with decreasing alloy purity. This observation was also made by Conrad, Okasaki, Badgil, and Jon[45] in titanium-oxygen alloys.

The tensile fracture strain data has been analyzed using a t test[33] to determine if the cooling rate significantly affects tensile ductility. For a given alloy purity and test temperature, the probability that the tensile ductility varies with cooling rate was always less than 80 percent. Thus, while the strain to fracture is not affected by cooling rate, the fracture toughness in some cases can be different by 30 percent. This result again points out the danger of trying to rate a materials toughness by smooth specimen ductilities.

The values of Young's modulus determined at 20°K are given in Table VIII and it is obvious that the modulus varies with alloy purity. A t test[33] was performed to compare the effect of cooling rate on E and with approximately 90 percent confidence, the Young's modulus of the furnace-cooled plate is significantly higher than that of the air-cooled material of the same purity.

While the tensile specimens were being tested, long bands of local surface roughness developed parallel to the tensile axis (longitudinal direction). These features can be observed in the air-cooled ELI specimen strained at 20°K shown in Figure 15. The bands were observed in specimens tested at all temperatures and seemed to be most intense in regions 180° away

TABLE VIII

YOUNG'S MODULUS (E) OF Ti-5Al-2.5Sn ALLOYS AT 20°K (-423°F)

(Values indicate mean and standard deviation)

Alloy	E (10^5 MN/m^2)	E (10^6 psi)
ELI, Air Cooled	1.25 ± 0.07	18.1 ± 0.1
ELI, Furnace Cooled	1.27 ± 0.07	18.4 ± 0.1
Normal Interstitial, Air Cooled	1.32 ± 0.07	19.2 ± 0.1
Normal Interstitial, Furnace Cooled	1.34 ± 0.07	19.4 ± 0.1

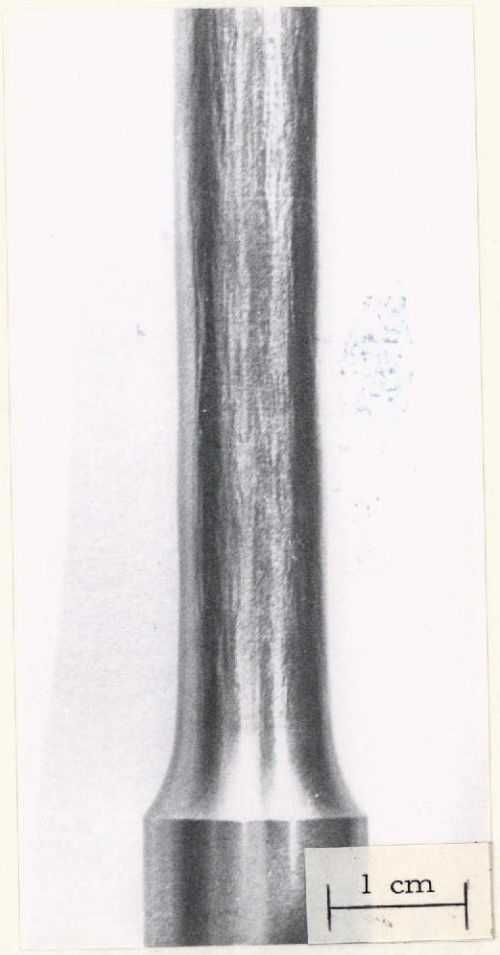

Figure 15. Photograph of the surface of a tensile specimen of the air cooled, ELI Ti-5Al-2.5Sn alloy which was strained at 20°K (-423°F).

from each other. The specimen orientation was marked on the 295°K and 77°K samples and it was observed that the bands formed on the side of the specimen which was perpendicular to the transverse direction. For that reason, it is believed that the surface roughness is closely related to the texture banding displayed in Figure 5. The roughness created no difficulty during testing and the specimen cross-section remained circular within the resolution of the point micrometer.

B. Ti-11.5Mo-6Zr-4.5Sn

The mechanical properties of this alloy were measured at room temperature for $\beta+\alpha$ and $\beta+\omega$ microstructures. In the α-aged condition (496°C or 925°F for 8 hours), the 0.2 percent offset tensile yield strength measured using longitudinal specimens was 1281MN/m^2 (185.7 ksi). An aging study on Beta III, ω-aged at 371°C (700°F) was carried out to find the aging time required to match the tensile yield strength of the α-aged material. Blocks of Beta III were ω-aged for 0.5, 1.0, 1.67, 3.0, 5.5, and 10 hours and two longitudinal tensile specimens were machined from each block. It was anticipated that this sub-β transus solution treated material would exhibit some tensile ductility in the ω-aged condition, but the first tensile specimen tested, which had been ω-aged for 0.5 hours, fractured before any perceptible macroscopic yielding behavior. Because of this, it became necessary to match the strength levels of α-aged and ω-aged materials on the basis of their compressive yield strengths. The compression specimens had a nominal diameter of 0.5 cm (0.2 inch) and a length-to-diameter ratio of four. The platens were lubricated with teflon and the 0.2% offset compressive yield strength was determined using the procedures described previously in this report.

Compression tests were performed using the material heat treated for the 371°C (700°F) ω-aging study. Those results are shown in Figure 16. The

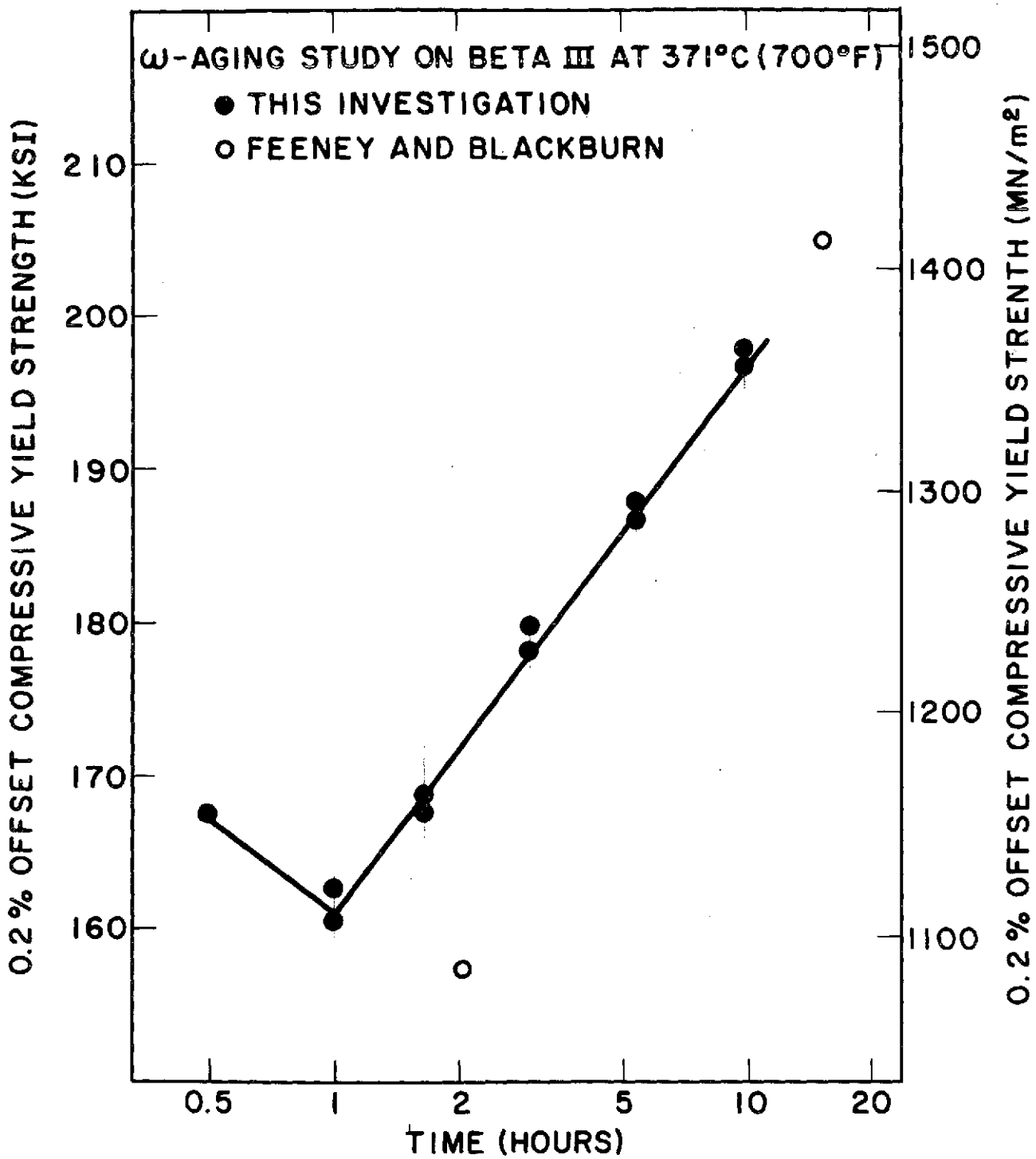

Figure 16. The variations of compressive yield strength of ω-aged Beta III with aging time at 371°C (700°F).

closed points represent individual specimen results from this investigation. The open points represent the results reported by Feeney and Blackburn[15] on super-β transus solution treated Beta III, ω-aged at 371°C (700°F). The reason for the elevated strength of the specimen aged for 0.5 hours is not known. Based on the data shown in Figure 16, a plate of Beta III was ω-aged at 371°C (700°F) for 3.5 hours to have a strength level similar to the β+α plate.

The tensile and compression specimens had longitudinal orientations. The plane strain fracture toughness was measured using 0.87 cm (0.75 inch) thick compact tension specimens with LT orientations. Thus, the applied load for both types of specimens acts parallel to the longitudinal direction. The average tensile, compressive, and fracture toughness properties of the Beta III determined to date are listed in Table VI along with their standard deviations. The individual specimen dimensions and K_{Ic} data for the α-aged Beta III material are given in Appendix A. No tensile or K_{Ic} tests have been completed on the ω-aged plate. The β+ω alloy is expected to exhibit no tensile ductility and its K_{Ic} is expected to be about 14.9 $MN/m^{3/2}$ (13.5 ksi$\sqrt{in}$) based on the maximum load and crack length of a K_{Ic} specimen which fractured during fatigue precracking.

The compressive yield strength of the α-aged Beta III is lower than the tensile yield strength. The probability that these test results are different as calculated from a t test[33] is greater than 95 percent, indicating the strength differential is a real effect. A previous investigation[13] comparing the tensile and compressive yield strengths on Beta III bar stock which was α-aged at 482°C (900°F) for 8 hours reported compressive yield strengths greater than the tensile yield strengths. The compression specimens used in that investigation had a nominal diameter of 1.25 cm (0.5 inch) and a length-to-diameter ratio of 2.5. No mention was made of platen lubrication. A specimen with

such a low aspect ratio and possibly without lubrication used during testing would tend to measure artificially higher compressive strengths with respect to the specimen and test conditions used in this investigation due to end effects. Thus, there is no known data that would make the observation of a lower compressive yield strength suspect.

The tensile flow curve of the α-aged Beta III is shown in Figure 17. The true stress is considered to be the flow stress because only a very small amount of necking is observed. The fracture strain (0.109) is smaller than the 0.12 strain required for use of the Bridgman correction in Equation (3). The values of σ_o, A, and m as determined by the empirical flow curve regression analysis and the statistical significance of the empirical curve are listed in Table VII. Again, the quality of the fit is excellent.

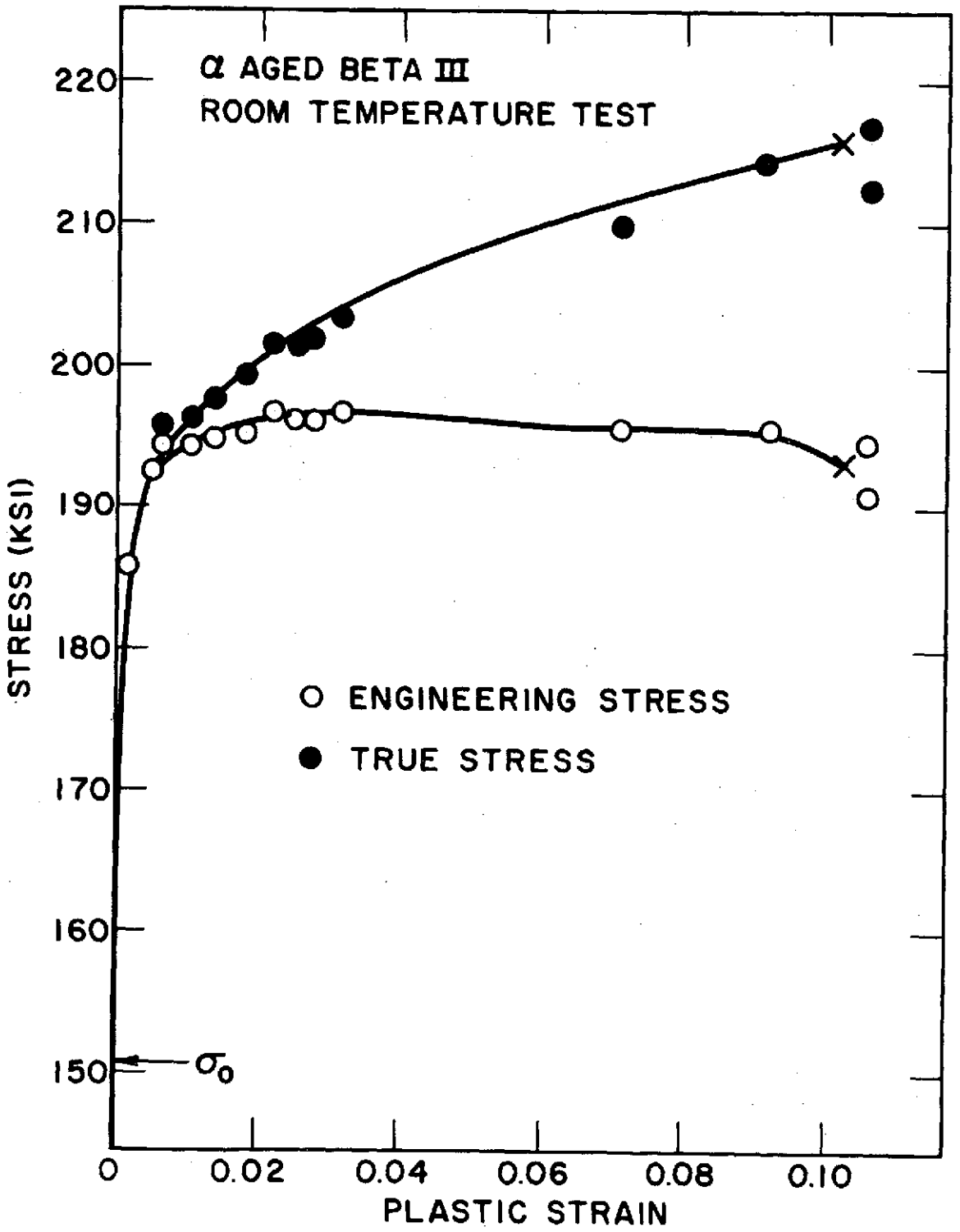

Figure 17. Room temperature tensile curves of α-aged Beta III. The solid true stress curve and σ_o are results of the regression analysis and "X" represents the average fracture strain.

FRACTOGRAPHY

The fracture surfaces were to be initially studied using transmission electron microscope (TEM) two-stage, platinum-carbon replicas. The fracture modes should be determined for all alloy composition, heat treatment, testing temperature, and specimen geometry combinations (36 different conditions). This task was never totally completed because certain changes in fracture modes became obvious. For example, the Ti-5Al-2.5Sn 1x1 LS and 1x1 LT fracture toughness specimens had the same fracture mode, and those of the 1x2 LT K_{Ic} specimen fracture surfaces would not be expected to be different, thus, substantially reducing the number of combinations to be studied. After the initial characterization, techniques similar to those used in quantitative optical metallography were to be used to measure the sizes and areal fractions of various fractographic features. The scanning electron microscope (SEM) was used to help with the quantitative fractography when the features were so large that only one or two of them could be observed when the TEM replicas were viewed at the lowest possible magnification (1700x). All fractographs were reviewed using stereo pairs. A stereo pair is a set of fractographs taken of the same region, but in one of them the specimen is tilted 6 degrees from its initial orientation. When viewed simultaneously with a stereo viewer, a fracture surface appears as a three-dimensional surface and small changes in the level, not noticed in a single fractograph,can be observed. All fractographs from the K_{Ic} specimens were taken of the region 2mm ahead of the fatigue crack so that these observations relate to the region which was deformed during the fracture toughness test prior to fast fracture. The progress made on characterizing the fracture surfaces will be discussed separately for each alloy.

A. Ti-5Al-2.5Sn

No attempt will be made to review the characteristics of the fracture surfaces of the Ti-5Al-2.5Sn alloys in all composition, cooling rate, testing

temperature, and specimen geometry combinations. Instead, examples of the types of features observed at each testing temperature will be noted.

Figure 18 shows TEM fractographs from tensile specimens of the air-cooled material of both grades of the α alloy which were broken at room temperature. Both of the materials fail by a fracture mode known as dimpled rupture. In dimpled rupture, microscopic voids nucleate at inclusions, precipitates, or some other microstructural feature. Upon further deformation, the voids grow and coalesce resulting in the final fracture. This mode of fracture occurs in most structural materials and though it requires large amounts of very localized plastic deformation, the fracture behavior from a macroscopic point of view is often very brittle. This fracture mode is also called microvoid coalescence or plastic fracture. The reason for the term dimpled rupture is that both sides of the fracture surface is covered by depressed regions, or dimples, which result from the void initiation, growth, and coalescence.

The air-cooled ELI room temperature tensile fracture surface (Figure 18a) contains dimples which are roughly equiaxed and have diameters of the order of 5 μm. In many of the dimples, evidence of a void initiation site usually below 1 μm in size can be observed. The room temperature tensile fracture surface of the air-cooled normal interstitial alloy (Figure 18b) also contains dimples, but they are often elongated with widths of about 6 μm and lengths two to three times the width dimension. Void initiation sites with sizes of 1 to 2 μm can be observed in many of the dimples. One of particular interest is noted by the arrow in Figure 18b. In the center of a large dimple (6 by 15 μm) a depression about 1 μm wide runs the length of the dimple and appears to start at the noted feature. The apparent void initiation site has a size similar to the iron-rich second-phase particles and it is believed that these particles are the void initiation sites. Other

dimples such as the ones noted by A also have these depressions but many equiaxed dimples are also observed. Thus, the room temperature fracture mode is dimpled rupture with two types of dimples. The elongated dimples are quite different than the equiaxed ones observed in classical dimpled rupture where roughly spherical voids grow around void initiation sites.

Examples of the fracture surfaces of fracture toughness specimens tested at 77°K (-320°F) are shown in Figure 19. Figure 19a shows a TEM fractograph for the furnace-cooled ELI material. Here there is no doubt that two populations of dimples exist. The ones in region A are equiaxed with a diameter 5 to 10 μm. Once again evidence of a submicron void initiation site could be observed in the bottoms of many of the dimples. The much larger dimples (20 to 30 μm) of region B are very shallow and rather featureless. They have shallow depressions about 5 μm parallel to their longest dimension. In this fractograph, there is no evidence of a void initiation site for the long, shallow dimples.

Figure 19b shows a TEM fractograph of the air-cooled normal interstitial alloy taken from a 77°K fracture toughness specimen. The areal fraction of the fracture surface covered with the long, shallow dimples is much greater in this alloy. These features, such as the ones shown in Region A, are parallel and the shallow depressions in the center of the dimples are aligned in the same direction. This morphology suggests that these features may be associated with a crystallographic deformation mode. The orientation of the long, shallow dimples in Region B is much different than Region A. There is a sharp boundary which seems to separate these regions. That boundary may be a grain boundary which separates grains of largely different crystallographic orientations. There are many smaller dimples near that boundary in Region C. The smaller dimples seem to end, permitting the

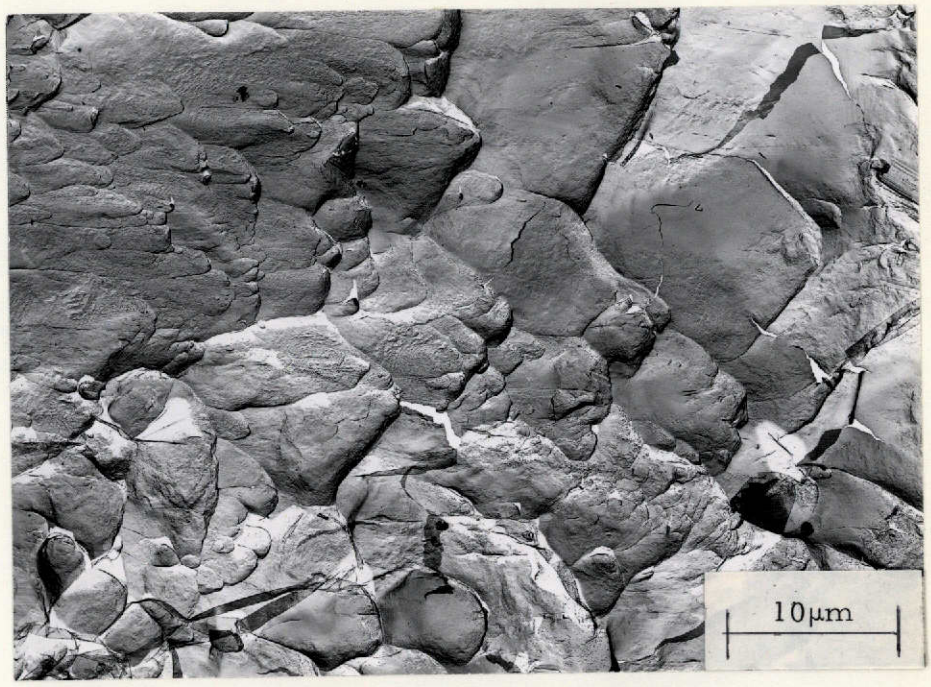

Figure 18a

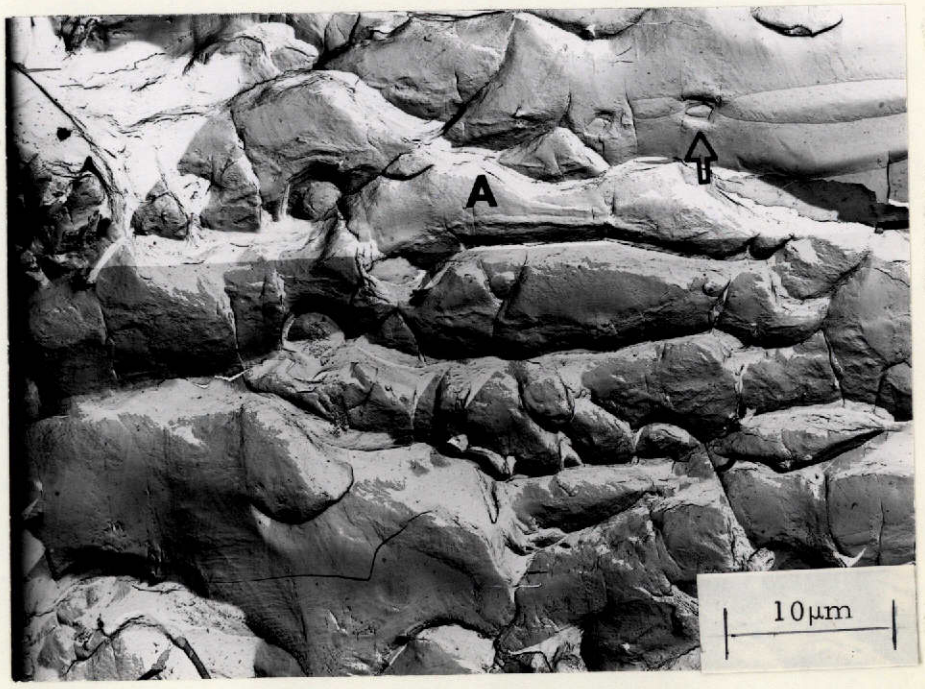

Figure 18b

Figure 18. TEM Fractographs of (a) air-cooled ELI and (b) air-cooled normal interstitial Ti-5Al-2.5Sn alloys from tensile specimen tested at room temperature. (Arrow points to a void initiation site and A indicates region of long, shallow dimples.)

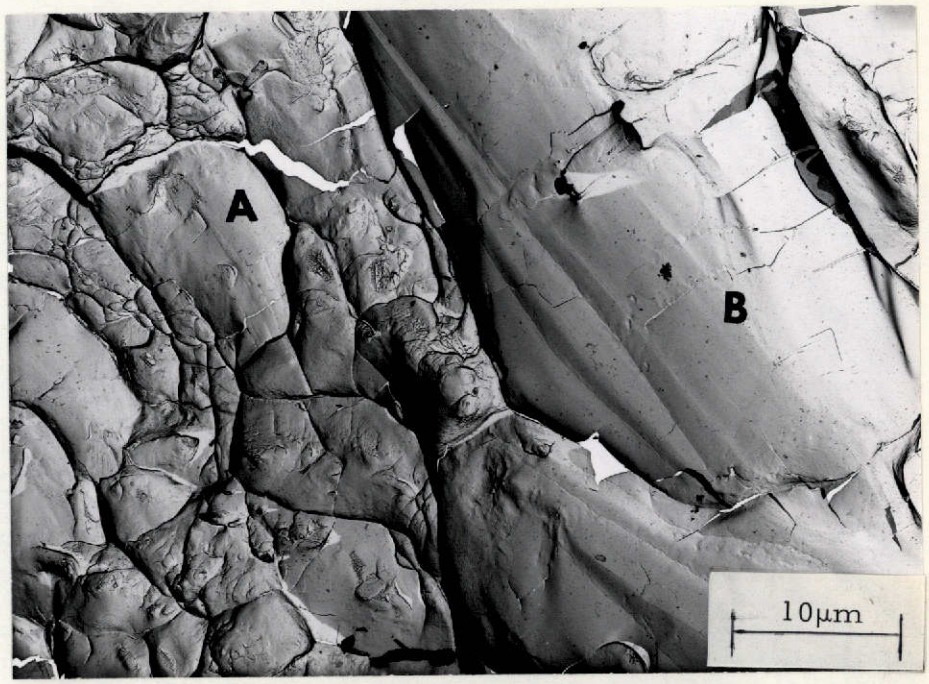

Figure 19a

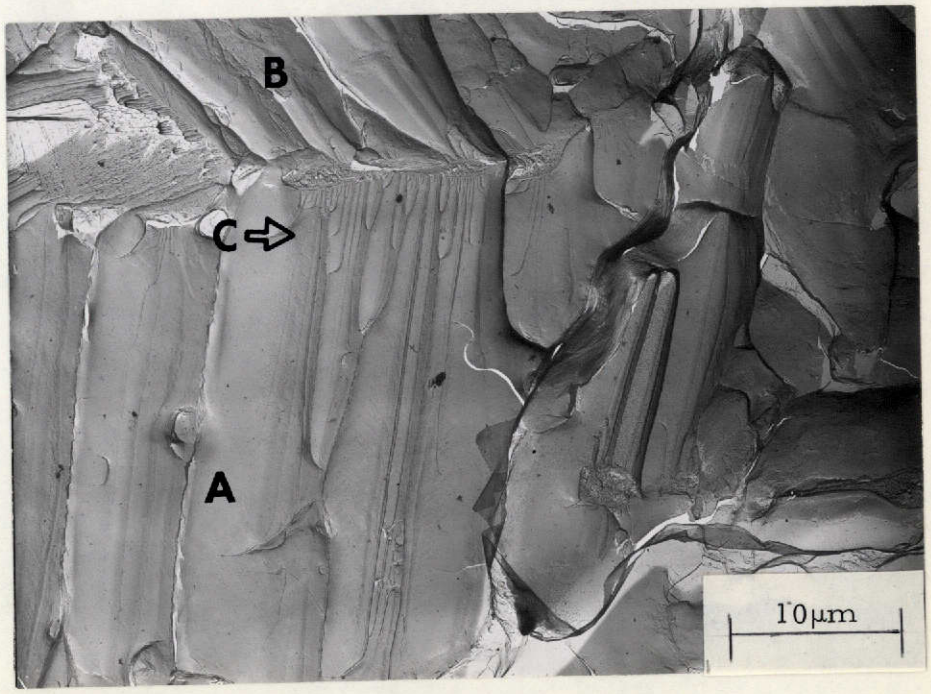

Figure 19b

Figure 19. TEM fractographs from K_{Ic} specimens tested at 77°K (-320°F). (a) Furnace-cooled, ELI Ti-5Al-2.5Sn. (A and B indicate region of equiaxed and long, shallow dimples, respectively.) (b) Air-cooled, normal interstitial Ti-5Al-2.5Sn. (A and B are regions of long, shallow dimples. C indicates a region of smaller dimples with river patterns.)

formation of the large, shallow dimples. When these regions are viewed in a single fractograph, one may get the impression that they are river patterns on a cleavage facet,[46] but observations of these regions with stereo pairs clearly reveals that they are shallow dimples. Wanhill[47] has observed similar features on the fracture surfaces of stress corrosion specimen of α titanium alloys and identified the fracture mode as cleavage. McMahon and Truax[4] have observed these features on stress corrosion fractures of α titanium and described them as long, finger-like grooves. That description could be used to describe the long, shallow dimples on the fracture surfaces of these Ti-5Al-2.5Sn alloys.

Figures 20 and 21 show TEM fractographs taken from the 1x1 LT fracture toughness specimens tested in liquid hydrogen. Figure 20a shows a fractograph of the furnace-cooled ELI alloy where a region of the long, shallow dimples is longer than 50 μm in length. Again the features are aligned in one direction and 1 μm wide depressions are in the bottoms of the long, shallow dimples. The river pattern-like features are also observed in the fractograph from the furnace-cooled, normal interestitial Ti-5Al-2.5Sn alloy shown in Figure 20b. At regions A and B, there appears to be some discontinuities in the shallow depressions along the center of the long dimples, but its source is unknown. In the regions labeled C in Figures 20a and 20b, the fracture mode is classical dimpled rupture. There were large regions of classical dimpled rupture present, especially in the ELI alloys. Figure 21 shows one such region in a TEM fractograph of an air-cooled ELI fracture toughness specimen. The average dimple diameter is about 5μm and in some of them a void initiation site could be observed. The initiation sites were smaller than 1 μm and a few of them are noted by arrows in Figure 21.

The fracture mode in the Ti-5Al-2.5Sn alloys was dimpled rupture, but two types of dimples were observed. The equiaxed dimples were 5 to 10 μm in diameter and in some of them void initiation sites could be observed. These sites had sizes similar to the iron-rich second-phase particles suggesting that they are the void initiating particles. The long, shallow dimples were about 6 μm long and were up to 50 μm long. They were rather featureless except for a shallow 1 μm depression along the length of the dimple. The sides and long dimple were aligned in one direction suggesting a crystallographic deformation process took part in the formation and growth of these features.

There seemed to be an increase in the fraction of the fracture surface covered by the long, shallow dimples in any condition where the fracture toughness was decreased. Reductions in K_{Ic} resulted from decreased testing temperatures, decreasing the alloy purity, and in the case of the ELI alloys, slower cooling rates from the annealing temperature. The change in fracture mode from classical dimpled rupture (equiaxed dimples) to non-classical dimpled rupture (elongated dimples) seemed to be a continuous transition. There seemed to be more of the long, shallow dimples on the K_{Ic} fracture surfaces than on tensile specimen fracture surfaces.

Williams and Pelloux[48] have observed features similar to the long, shallow dimples in α titanium alloys. By studying mating fracture surfaces with stereo pairs, they concluded that the observed features were not dimples on both sides of the fracture surface. One side of the fracture was dimpled, but the other side contained upraised matching regions. If this is the case in the Ti-5Al-2.5Sn alloys when fractographs are viewed in stereo pairs, some of the long, shallow features should be depressed and others should be raised on the same fractograph. This was never observed in the TEM fractographs, but lower magnification scanning electron

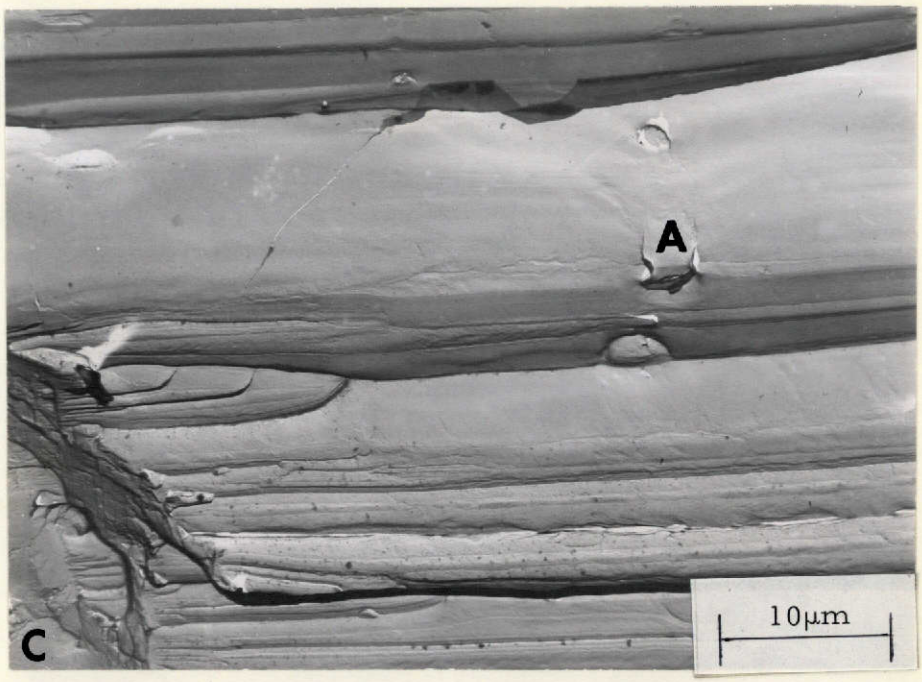

Figure 20a

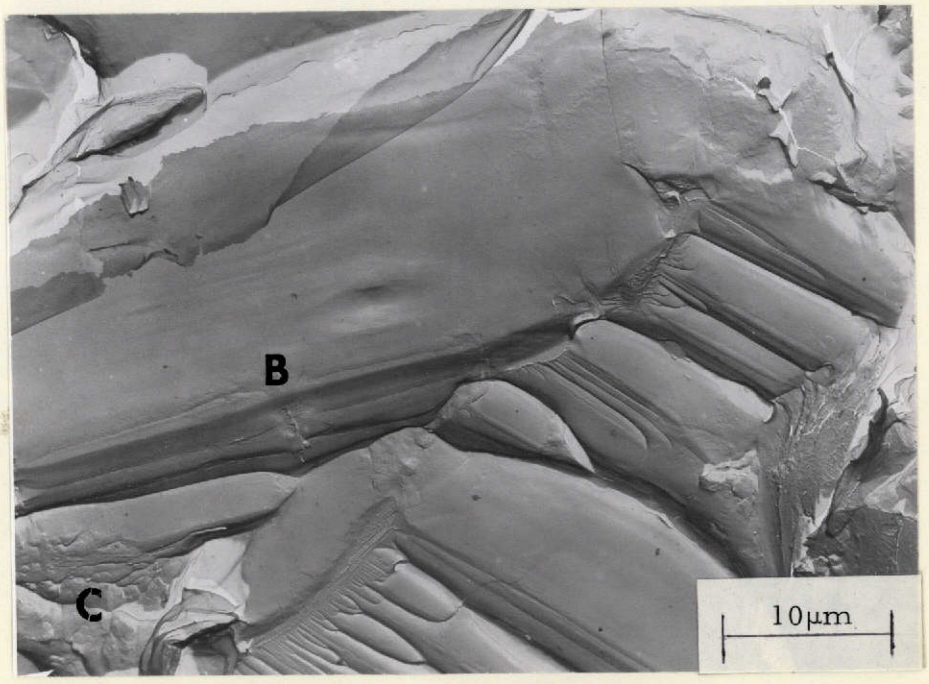

Figure 20b

Figure 20. TEM fractographs from 1x1 LT bend K_{Ic} specimens tested at $20^{o}K$ ($-423^{o}F$). (a) Furnace-cooled, ELI Ti-5Al-2.5Sn. (b) Furnace-cooled, normal interstitial Ti-5Al-2.5Sn. (A and B are regions of discontinuities in the long, shallow dimples and C indicates regions of classical dimpled rupture.)

Figure 21. TEM fractograph of the air-cooled, ELI Ti-5Al-2.5Sn alloy from an LT orientated 1x1 bend K_{Ic} specimen tested at 20°K (-423°F). (Arrows point to void nucleation sites.)

microscope fractography is now being used to observe the contours of these regions. From observations made to date, it is believed that these features are all dimples.

Further study of the fracture mechanism of the Ti-5Al-2.5Sn alloys was restricted to the fracture process at the temperature of liquid nitrogen ($77^{o}K$). Within a given alloy, there seemed to be little change in the fracture mode between $77^{o}K$ and $20^{o}K$. If a difference existed, it was only a matter of the degree of change. It is felt that the effect of microstructure on the fracture toughness at $77^{o}K$ will be very similar to the effect at $20^{o}K$. Study of the fracture mechanism at $77^{o}K$ has the additional benefit of being much less difficult experimentally than a similar study at $20^{o}K$.

Because of the large size of the long, shallow dimples, the liquid nitrogen fracture surfaces of the Ti-5Al-2.5Sn alloys are being studied using the scanning electron microscope (SEM) at a magnification of 500x. Quantitative fractography will be used to determine the areal fraction and size of the long, shallow dimples from tensile and K_{Ic} specimen fracture surfaces. The possible differences between the fracture modes in tensile and fracture toughness specimens are very important because of their effect on the sectioning study. In that study, both tensile and K_{Ic} specimens will be plastically strained, metallographically sectioned, and studied to observe the development of the fracture process. It is far more desirable to study tensile specimens rather than K_{Ic} specimens for reasons which will be described later in this report. If through quantitative fractography, no difference in fracture mode is observed with specimen type, the results of sectioning experiments on tensile specimens will be useful in making suggestions on the improvement of fracture toughness. If a difference is observed, both tensile and K_{Ic} specimens must be sectioned.

The quantitative fractography has not yet been completed, but the SEM fractographs taken for that study will be presented and discussed. For each alloy, a fractograph from a tensile and K_{Ic} specimen will be shown. In the K_{Ic} fractographs, the macroscopic direction of crack propagation will be from left to right. Because of the lower magnification and nature of the SEM, much of the detail shown in the TEM fractographs will not be observed. All SEM fractographs were taken using the image from the secondary electrons.

Figure 22 shows the SEM fractographs of the air-cooled ELI alloy tested at 77°K. The tensile fractograph (Figure 22a) shows a large portion of the fracture surface covered by classical dimpled rupture. The long, shallow dimples appear to be about 15 μm wide and 35 μm long. The K_{Ic} fractograph (Figure 22b) shows a much larger fraction of the fracture surface covered by the long, shallow dimples, which have sizes similar to those in tensile specimens. Two of these features with a slight angle between them can be observed at Region A. This pattern was observed frequently and may be related to the crystallography of a deformation process.

The SEM fractographs for the furnace-cooled ELI alloys are shown in Figure 23. The tensile fractograph (Figure 23a) has less classical dimpled rupture than the air-cooled ELI tensile fractograph. The size of the long, shallow dimples seems to be independent of cooling rate from the annealing treatment. The K_{Ic} fracture surface (Figure 23b) is almost completely covered with the non-classical dimpled rupture mode. There seems to be a tendency for these features to be narrower (10 μm) but with similar lengths to the long, shallow dimples in the other ELI conditions. Evidence of the second phase are indicated by arrows and seems to lie in the bottom of the long, shallow dimples.

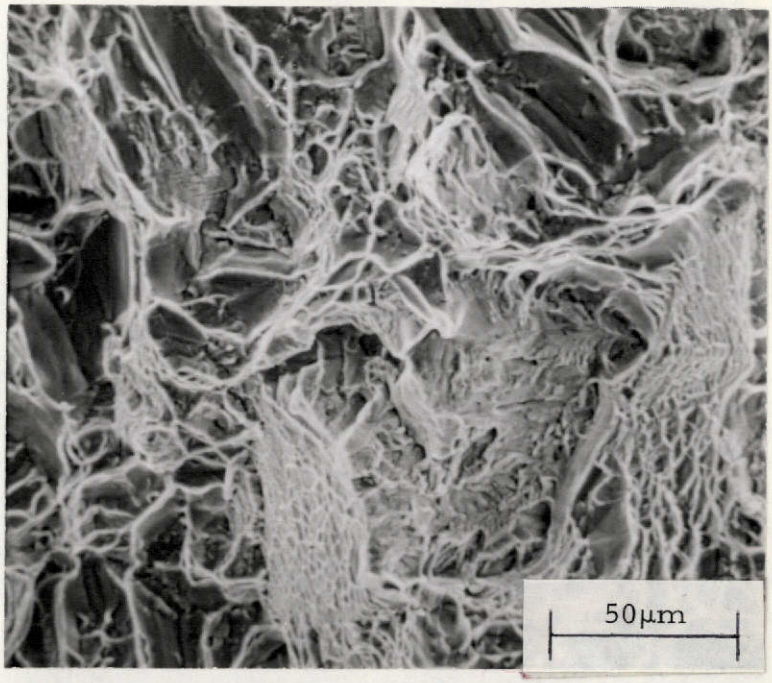

Figure 22a

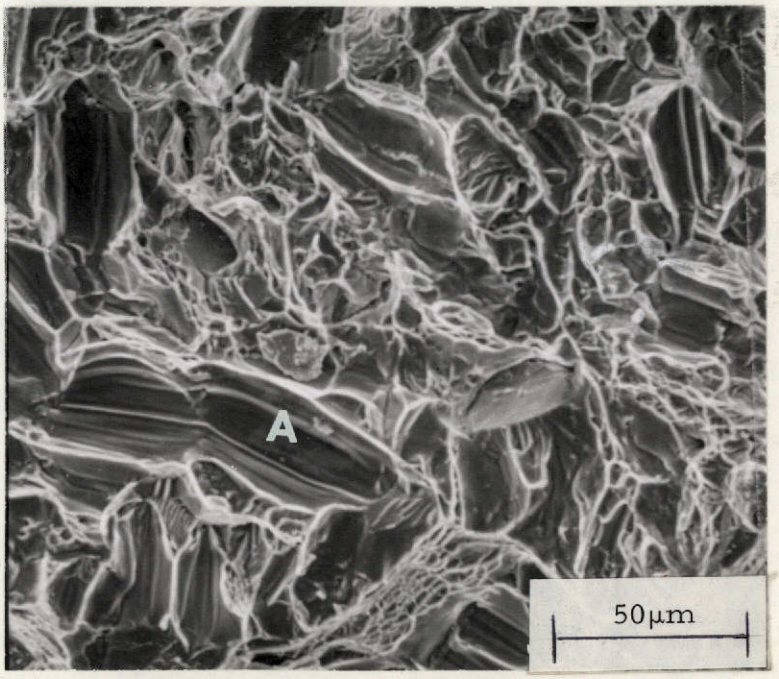

Figure 22b

Figure 22. SEM fractographs of the air-cooled, ELI Ti-5Al-2.5Sn alloy from (a) tensile and (b) K_{Ic} specimens tested at 77°K (-320°F). (A indicates a long, shallow dimple.)

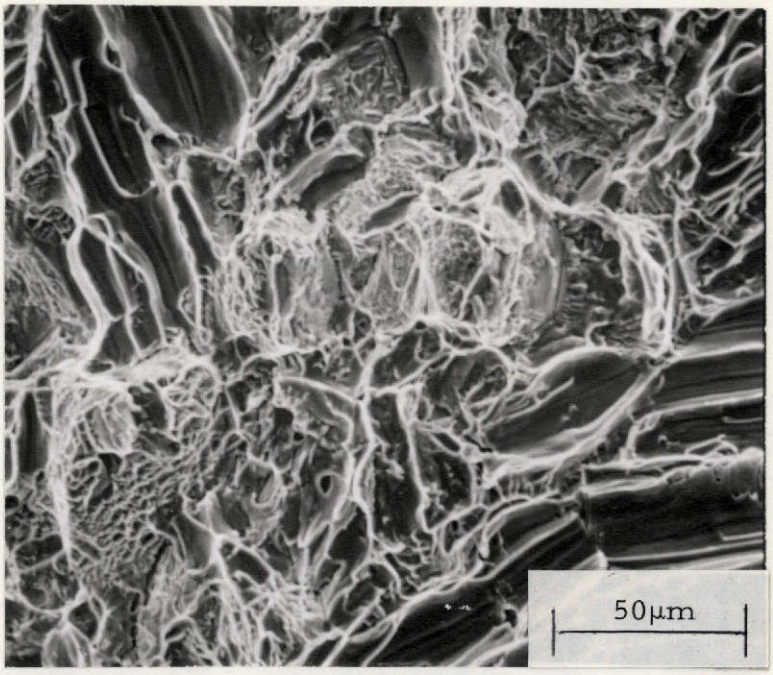

Figure 23a

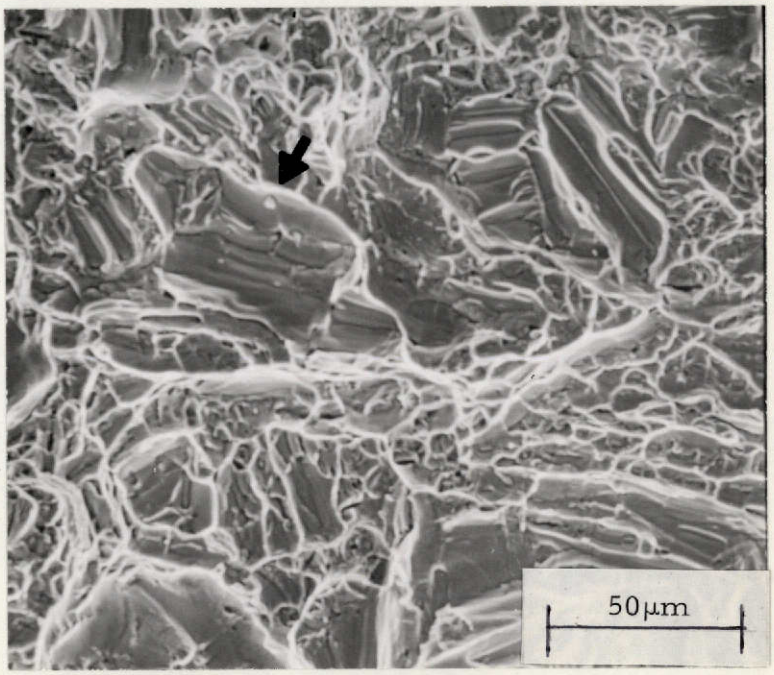

Figure 23b

Figure 23. SEM fractographs of the furnace-cooled, ELI Ti-5Al-2.5Sn alloy from (a) tensile and (b) K_{IC} specimens tested at 77°K (-320°F). (Arrow points to a void nucleation site.)

Figure 24 shows the SEM fractographs of the air-cooled, normal interstitial material tested at 77°K. A large portion of the tensile fracture surface (Figure 24a) is covered by the long, shallow dimples, which are about 5 μm wide and 30 μm long. In almost every dimple, there is evidence of a void initiation site along the narrow depression in the center of the long dimples. These sites are several micrometers in size suggesting it may be the iron-rich second-phase. The K_{Ic} fracture surface (Figure 24b) is similar to that of the tensile specimen. In this fractograph, it is clear that the long dimples form in patches often 25 μm in size. Region A shows such a patch which is 75 μm long, twice this alloy's average grain size.

Typical SEM fracture surfaces from the furnace-cooled, normal interstitial specimens are shown in Figure 25. Both the tensile and K_{Ic} fracture surfaces are similar to those described for the air-cooled, normal interstitial material.

From the SEM fractographs, it is clear that as the toughness decreases, more of the long, shallow dimples appear on the fracture surface. The possible difference between the tensile and K_{Ic} fracture mode is unclear at this point. Upon completion of the quantitative fractography, some of the uncertainties will become clearer.

B. Ti-11.5Mo-6Zr-4.5Sn (Beta III)

The fracture surfaces of both tensile and K_{Ic} specimens of the $\beta+\alpha$ and $\beta+\omega$ microstructures are to be investigated using techniques similar to those described for the Ti-5Al-2.5Sn alloys. Of particular interest is the difference in fracture modes between tensile and K_{Ic} specimens for α-aged Beta III. The metastable β titanium alloys have the unique characteristic that changes in processing and heat treatment can result

in increased tensile ductility while the fracture toughness is reduced.[49] No observations of the fracture surfaces of ω-aged Beta III have been made using electron beam instruments, but the fracture surface from the specimen which fractured during precracking was examined with an optical microscope.

TEM fractographs taken from tensile and K_{Ic} specimens of the α-aged material are shown in Figure 26. The fracture mode is classical dimpled rupture in both cases. The tensile fracture surface (Figure 26a) contains equiaxed dimples about 3 μm in size. In some of the dimples, a nucleation site of about 0.2 μm in size could be observed. The K_{Ic} fracture surface (Figure 26b) has two size distributions of equiaxed dimples. The larger ones are about 4 μm in diameter and had a void initiation site of about 0.5 μm. The small dimples are about 1 μm in diameter and 0.1 μm void initiation sites were observed. It was difficult to clearly observe the void initiation sites without the use of stereo pairs. In α-aged Beta III, the void initiation site in the large dimples is believed to be the primary α particles, while the small dimples on the K_{Ic} fracture surfaces are believed to be nucleated at the smaller α precipitates. These suggestions are based on the relative sizes of these precipitates which were displayed in Figure 9.

The fracture surface of the ω-aged Beta III specimen which fractured during fatigue precracking was observed using an optical stereomicroscope. The fracture surface was very flat, however facets could be observed at low magnifications. These facets had a striking resemblance to the etching bands in the solution treated Beta III which were shown in Figures 6 and 8. When viewed at higher magnifications, there appeared to be a series of parallel lines on each facet. These observations are very similar to those of Chesnutt and Williams[50] on ω-aged Beta III. They showed that the facets were covered by very small equiaxed dimples. Further fractographic study of this alloy will be performed using electron beam instruments.

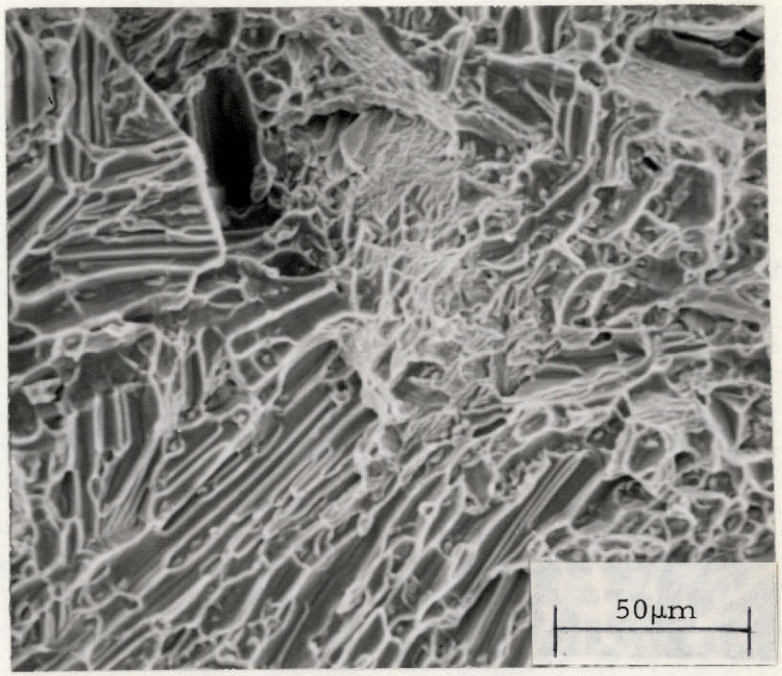

Figure 24a

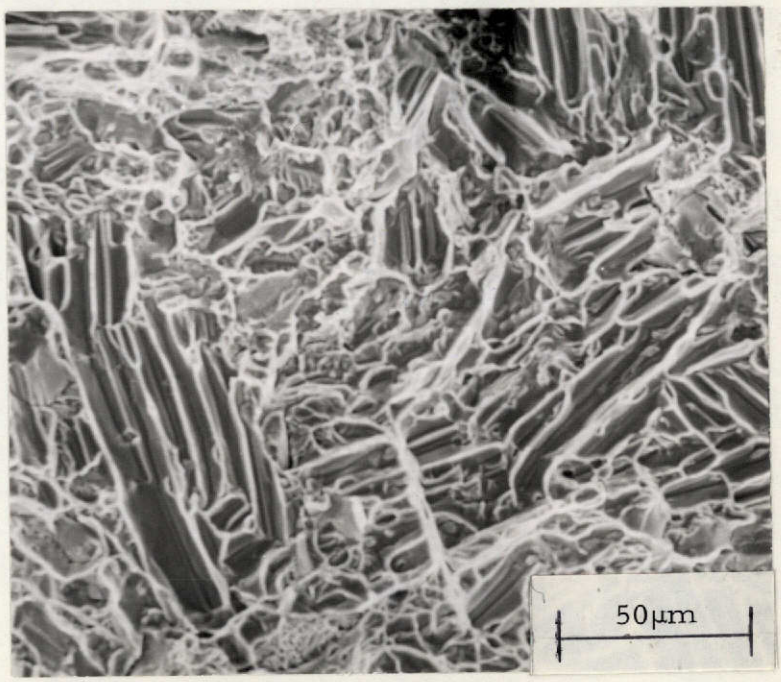

Figure 24b

Figure 24. SEM fractographs of the air-cooled, normal interstitial Ti-5Al-2.5Sn alloy from (a) tensile and (b) K_{Ic} specimens tested at 77°K (-320°F). (A indicates region of long, shallow dimples.)

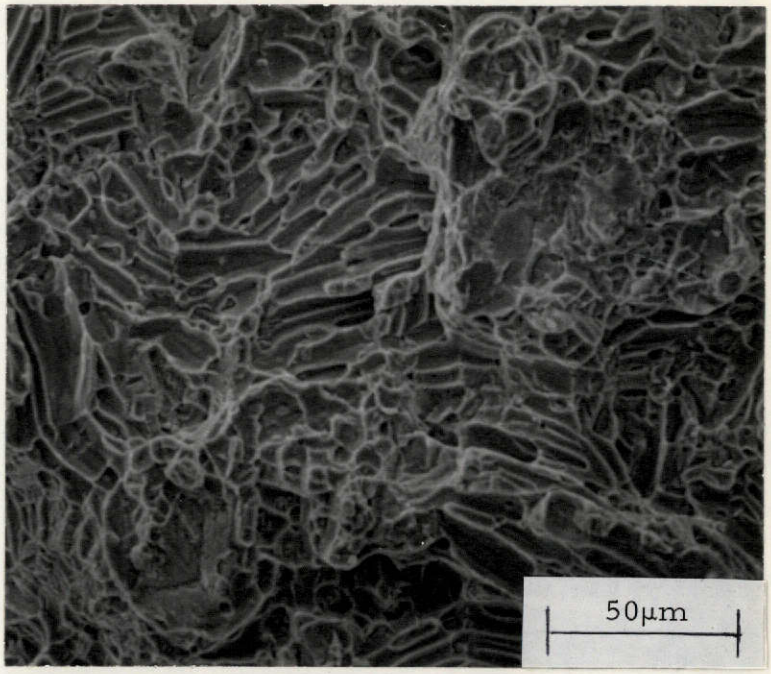

Figure 25a

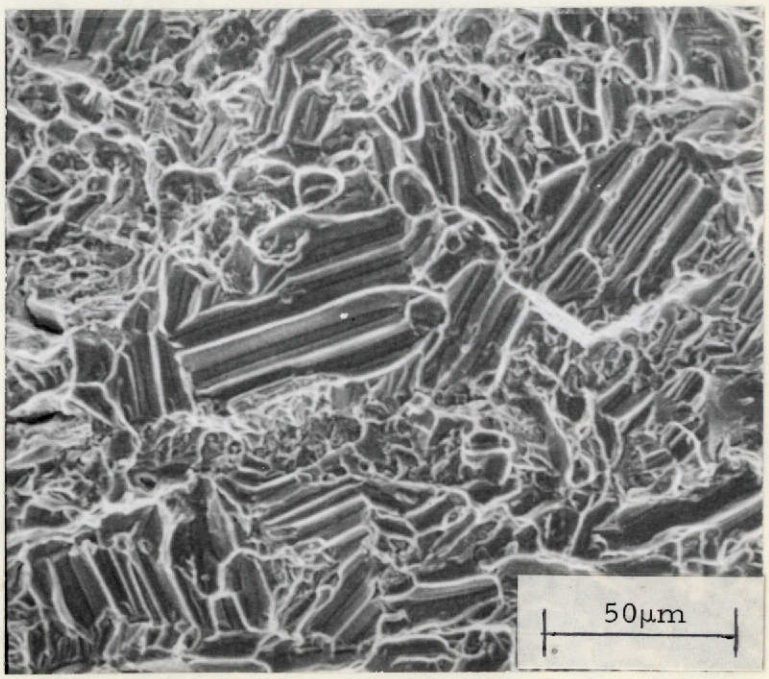

Figure 25b

Figure 25. SEM fractographs of the furnace-cooled, normal interstitial Ti-5Al-2.5Sn alloy from (a) tensile and (b) K_{Ic} specimens tested at 77°K (-320°F).

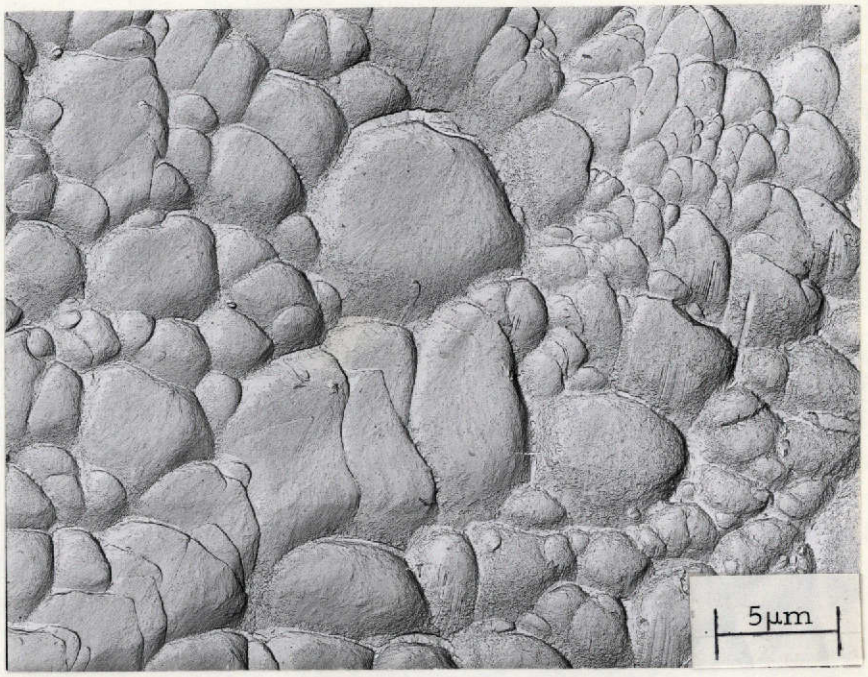

Figure 26a

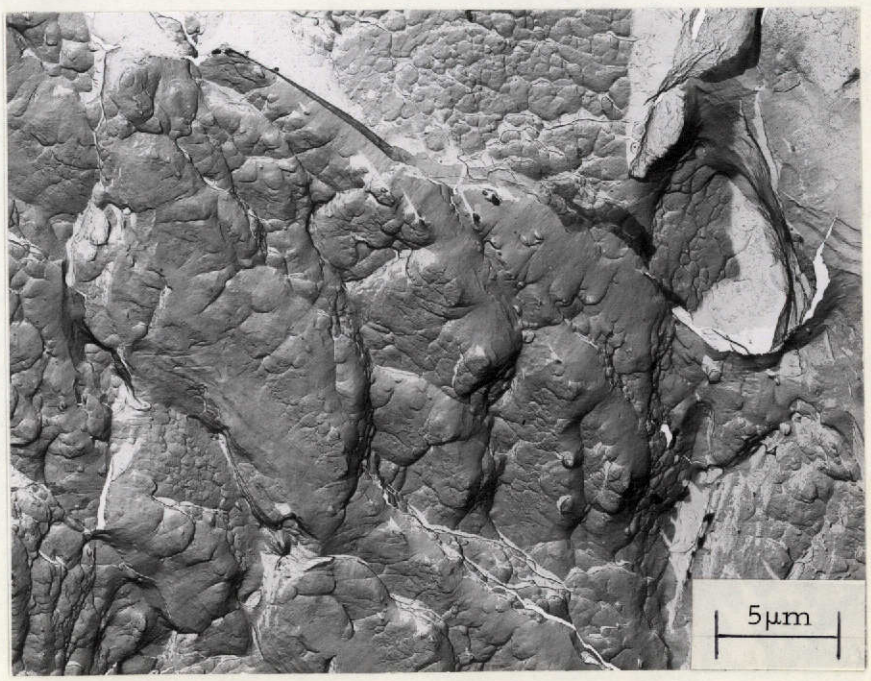

Figure 26b

Figure 26. TEM fractographs of α-aged Beta III from (a) tensile and (b) K_{Ic} specimens tested at room temperature.

DISCUSSION OF RESULTS AND FURTHER WORK

Based on the evidence presented above and work which has been previously reported,[1] proposed fracture mechanisms for the Ti-5Al-2.5Sn alloys and α-aged Beta III will be discussed along with further work which will be required to clarify the exact fracture mechanisms. It should be pointed out that the models presented here are the best estimates of how fracture occurs in these alloys and many details of the fracture mechanisms are uncertain at this time.

A. Ti-5Al-2.5Sn

Any fracture mechanism of the Ti-5Al-2.5Sn must include explanation of the six general observations made about the mechanical properties and fracture modes. First, the reason for the shape of the long, shallow dimples must be understood. The source of the river patterns and shallow depressions must also be explained. Second, why do α-alloys with decreased K_{Ic} have more of the long, shallow dimples? Third, the reason that normal interstitial alloys always have lower K_{Ic} than the ELI alloys must be known. Fourth, one must understand the change of K_{Ic} with cooling rate in ELI alloys as well as the absence of that effect in normal interstitial alloys. Fifth, the occurance of orientation effects on K_{Ic} in the ELI alloys must be explained. The cause for the absence of that effect in the lower purity alloys must also be known. Sixth, why do the fracture surfaces of K_{Ic} specimens seem to have more long, shallow dimples than the tensile specimens, especially for the tougher alloys?

The model which will be presented is based on the concept that the long, shallow dimples form at mechanical twin boundaries and changes in microstructure and stress state which increase local stress concentrations will result in more twinning and thus more non-classical dimpled rupture. Previously reported work on these alloys[1] include metallographic sectioning

of a fractured tensile specimen ($\varepsilon = 0.304$) of the air-cooled, normal interstitial alloy tested at 77°K. Several types of voids which formed in that specimen are shown in Figure 27. In these micrographs, the tensile axis and longitudinal direction is vertical and the transverse direction is horizontal. Figure 27a shows a grain which has deformed by both primary and secondary twinning and voids have formed along the interfaces between these twins. The individual voids have elliptical cross-sections with the longest dimensions of about 10 μm. Figure 27b shows two second-phase particles which have cracked surfaces perpendicular to the tensile axis. Figure 27c shows two particles which are on the surface of the same void. The morphology of the void is similar to that shown in Figure 27a suggesting that twinning played a role in the void formation. An arrow in Figure 27c points to a twin which has formed ahead of the void. Thus, it appears that two competing fracture processes are occuring in the Ti-5Al-2.5Sn alloys. One is the nucleation of voids at the iron-rich particles (classical dimpled rupture) and the other is void nucleation at twin boundaries (non-classical dimpled rupture). During this discussion, attention will be given to the twin nucleated voids because decreases in K_{Ic} are associated with increasing amounts of non-classical dimpled rupture.

The voids which form at the twin boundaries are believed to correspond to the long, shallow dimples on the fracture surfaces. Their parallel alignments suggested that a crystallographic deformation mode such as twinning took part in the fracture process. Although no evidence exists for the source of the central depressions, it is believed that they form at the intersection of the primary and secondary twins. This void can then grow as a long, cylindrical void to the length of the intersection of the two twins. Upon further plastic deformation, the void will grow along a twin interface. The reason for growth along this boundary is not known, but may be related

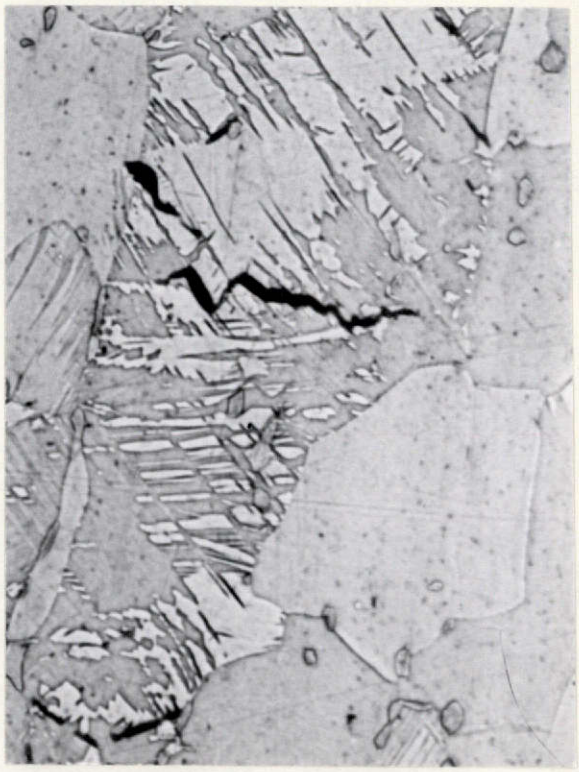

Figure 27a

Figure 27b

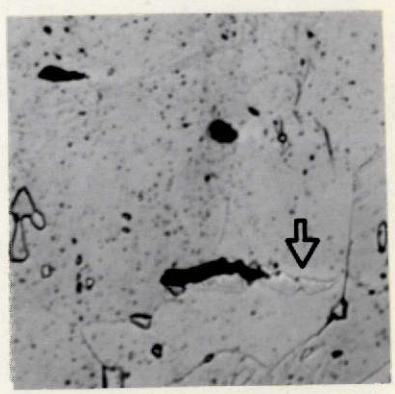

Figure 27c

50μm

Figure 27. Void initiation in a 77°K (-320°F) tensile specimen of the air-cooled, normal interstitial Ti-5Al-2.5Sn alloys at (a) twin boundaries, (b) cracked iron-rich particles, and (c) a twin (as indicated by the arrow) with two particles. (The tensile axis is vertical.)

to the many accommodation dislocations which have been observed at α titanium twin boundaries using thin foil TEM.[6] The many small, shallow dimples and river patterns may be a result of the size distribution of the primary and secondary twin interfaces.

The reason why these twin nucleated dimples reduce fracture toughness with respect to that measured when the fracture mode is classical dimpled rupture is unclear at this time. If the long, shallow voids grow very rapidly along the twin boundary, it would not be surprising for that process to absorb much less energy than the process of nucleation and growth of several equiaxed dimples 5 to 10 μm in diameter. It is obvious that more detailed knowledge is required about the formation of these possibly twin related features.

The critical question is what controls twinning in α titanium. Deformation twinning occurs in titanium so that extension or contraction can occur along the c-axis. The only other known deformation mode by which this can occur is <c+a> or $<11\bar{2}3>$ slip.[6,7] From investigations made to date,[7] it is not clear whether twinning or <c+a> slip is more likely during tensile deformation. Reed-Hill[51] has shown that the twin system which operated in zirconium, a hexagonal close-packed metal having lattice parameters almost identical to titanium, is the system with the highest resolved shear stress acting on it. Thus, twinning appears to occur based on a critical resolved shear stress criterion. One must now consider the the role of microstructure and mechanical stress concentrations such as cracks in causing local stresses high enough to activate twin systems.

One source of a stress concentration is a dispersed second phase. Continuum elastic stress analyses[52,53] indicate the stress concentration at a particle is independent of its size, but Ashby[54] has presented a dislocation model of a rigid particle in a slip band where the shear stress

component from the slip band is proportional to the particle diameter. According to this model, a larger particle will have a larger localized stress concentration associated with it. If this concept is applied to the Ti-5Al-2.5Sn alloys, one would expect more twinning in the normal interstitial alloys because of the higher stress concentrations associated with the larger size of the iron-rich second-phase particles. The higher oxygen contents of these alloys would also cause the dislocation arrays to be more planar[4-7] promoting higher stress concentrations. On the other hand, increasing the oxygen content in titanium alloys reduces the amount of twinning which is observed.[6-8] The point that increasing the size and volume fraction of the iron-rich second phase in these alloys causes drastic reductions in K_{Ic} is supported by the work of Erbin[55] on Ti-5Al-2.5Sn alloys of similar interstitial contents but varied iron levels. The toughness, measured using the ratio of the strength of a mildly notched sheet to the tensile yield strength, was drastically reduced in alloys with iron contents in excess of 0.2 weight percent, especially at cryogenic temperatures. The iron contents of the two grades studied here are 0.15 and 0.30 weight percent.

The next point needing to be explained is the effect of cooling rate on the fracture toughness of the ELI alloys. The furnace-cooled ELI alloys had a lower K_{Ic} and a large portion of its fracture surface was covered with the long, shallow dimples. Furnace cooling from the annealing temperature may be slow enough to cause ordering, which is common in titanium-aluminum alloys. The precipitation of the long range ordered phase α_2 has never been observed using thin foil TEM in Ti-5Al-2.5Sn alloys,[10,11] but Namboodiri, McMahon, and Herman[3] have suggested that short range order (SRO) can occur in a titanium-4 weight percent aluminum alloy. Their conclusion is based on the observation that

the electrical resistivity of that alloy passed through a minimum with increasing room temperature deformation. Dislocation motion destroys local order[56] and this may result in a reduction in resistivity. Further deformation causes increases in resistivity normally associated with work hardening. This effect was observed in specimens water-quenched from the 850°C (1562°C) annealing treatment but was much more noticeable in the specimens that were annealed, quenched, and then aged at 450°C (842°F), 550°C (1022°F), and 575°C (1067°F) for times in excess of 200 hours. Although this type of behavior is often associated with SRO, it is not an unambiguous characteristic of local order. Small angle scattering x-ray diffraction is the only way to clearly determine the presence of SRO. Several investigators[2, 57] have suggested that SRO occurs in titanium-aluminum alloys, but the work of Namboodiri, et al. is the best indirect evidence to date. No small angle scattering x-ray diffraction is known to have been done on titanium-aluminum alloys; but in the titanium-indium system, one with phases and structures similar to those in Ti-Al,[58] some x-ray work has been completed. Munster and Sagel[59] observed SRO in a titanium-6.9 atomic percent indium alloy and there was an excess of unlike nearest neighbor atoms. If the behavior in the Ti-5Al-2.5Sn alloys is similar to the Ti-In alloy, SRO would result in a greater frequency of Ti-Al nearest neighbor pairs. Statistical analysis of the Young's modulus data determined for the Ti-5Al-2.5Sn alloys at 20°K showed that the modulus of the furnace-cooled alloys is significantly greater than that of the air-cooled material of the same grade. Young's modulus is dependent upon the strengths of the interatomic bonds and the changes in elastic properties described above indicate that the cooling rate changes the types of interatomic bonds. Ogden, Markuth, Finlay, and Jaffee[60] reported that increasing the aluminum content increases the Young's modulus of Ti-Al alloys. Thus, increasing the number of titanium-aluminum nearest neighbor pairs increases Young's

modulus. The changes in Young's modulus observed in the Ti-5Al-2.5Sn suggest that SRO with an excess of unlike nearest neighbors occurs in the furnace-cooled alloys.

Typical characteristics of local order include more planar dislocation and dislocation pairs.[61] The first dislocation which passes over the lattice plane will require a higher stress to destroy the local order. The second dislocation will be able to move at a lower stress and will closely follow the first dislocation resulting in a pair. These changes in dislocation arrays can cause higher stress concentrations and thus promote twinning.

There are some indications of short range order in the literature of Ti-5Al-2.5Sn alloys. Shannon and Brown[12] measured the strength of smooth and sharply notched ELI Ti-5Al-2.5Sn sheet specimens at 20°K after being either stretched or rolled at room temperature. The material used was heat treated to two different conditions--annealed at 815°C (1500°F) and furnace-cooled or annealed at 760°C (1400°F) and air-cooled. Upon stretching, the air-cooled material showed no change in notched strength; but in the furnace-cooled condition, the notched strength increased by about 35 percent when it was stretched up to 12 percent. In both cases, there were only modest increases in yield strength upon stretching. This suggests that SRO, which may have caused the reduction in the toughness of the furnace-cooled sheet, was destroyed by dislocation motion during the stretching operation. It was also noted that rolling did not affect the toughness of these sheets. In titanium alloy sheet, there often exists intense basal textures,[31] so a large portion of the rolling deformation which would require contraction parallel to the c-axis may occur by twinning. This deformation mode is a rotation of the matrix and will not disrupt the nearest neighbor pair distribution or local order.

Dessau and Harris[62] reported the liquid hydrogen K_{Ic} of ELI Ti-5Al-2.5Sn forgings. After forging, the material was vacuum annealed at 760°C (1400°F), cooled by a helium purge to 538°C (1000°F) in less than 10 minutes, furnace-cooled to 149°C (300°F), and air-cooled to room temperature. The microstructures of the forgings as observed in the light microscope were similar to those of the ELI plate studied here and the 20°K fracture toughness was similar to that of the furnace-cooled ELI plate. The initial helium purge cooling rate was similar to that of the air-cooled plate, but this was followed by furnace cooling. Thus, furnace cooling below 538°C (1000°F) seems to reduce the toughness. Namboodhiri, et al.[3] observed large decreases in electrical resistance of deformed specimens aged in this temperature range, suggesting the formation of local order.

Curtis, Boyer, and Williams[10] reported the room temperature toughness of normal interstitial Ti-5Al-2.5Sn plate heat treated in various conditions. The toughness was measured using fatigue cracked specimens; but in most conditions, the specimens were too thin to determine a valid K_{Ic}. Decreases in annealing temperature and cooling rates resulted in drastic reductions in apparent toughness but with little change in yield strength. Thin foil TEM selected area diffraction gave no spots indicating α_2 precipitation even though the plate was aged between 500°C (932°F) and 538°C (1000°F) for 128 hours. The toughness of this material was about 35 percent lower than a specimen given the same annealing treatment, 760°C (1400°F) for 2 hours, and air-cooled. This again points out the danger of having Ti-5Al-2.5Sn alloys near 538°C (1000°F) for long periods of time. A fractograph of a stress corrosion failure of annealed and air-cooled material showed a long, shallow dimple, but no mention was made of the fracture mode in specimens tested in air. The relationship between these

room temperature toughness results and the formation of the long, shallow dimples which occur most frequently at cryogenic temperatures is not clear.

Thus, slow cooling promotes losses in toughness and it is believed to be associated with short range order. The question now becomes why this effect was not observed in the normal interstitial plates. It is entirely possible that the stress concentration arising from local order are small relative to those of the large dispersed phase and thus their effect in the normal interstitial effect may not be observed in gross mechanical properties tests like K_{Ic}.

The reason for the variation of fracture toughness with specimen orientation in the ELI alloys is not clear but may be related to the crystallographic texture shown in Figure 5. If twinning occurs based on a critical resolved shear stress criteria as previously suggested, the specimen orientation and crystallographic texture will affect the resolved shear stress acting on a given twin system. Until the twin systems which operate in Ti-5Al-2.5Sn are identified, no prediction of K_{Ic} with specimen orientation can be made. The absence of orientation effects in the normal interstitial material cannot be fully explained until the texture of these plates are determined.

The cause of more non-classical dimpled rupture in the K_{Ic} specimens may be the high stress concentrations at the tip of the fatigue crack in contrast to the relatively uniform stress state in a tensile specimen.

This model is based on the concept that voids can form at twin boundaries such as those shown in Figure 27. Any macrostructural or microstructural feature which will increase the resolved shear stress acting on a twin system, whether it be a dispersed phase, local order, crystallographic texture, or a macroscopic crack, will tend to increase the amount of

twinning and thus the amount of long, shallow dimples observed on fracture surfaces. It has been shown that as more of the non-classical dimpled rupture is observed, the fracture toughness is reduced. All known information about composition, heat treatment, microstructure, fracture toughness, and fracture mechanisms of α titanium alloys with equiaxed grains is consistent with this model. It suggests that the fracture toughness of Ti-5Al-2.5Sn alloys may be improved by reducing the size of the iron-rich second-phase particles, reducing the amount of local order by using relatively high annealing temperatures and rapid cooling rates, and reducing the α grain size. The last factor will reduce the amount of twinning which will occur at a given strain level.[63] According to the model, the role of oxygen is unclear. Oxygen increases the intensity of slip bands and simultaneously reduced the amount of twinning observed. Based on the work of Okazaki, Morinaka, and Conrad[64] on grain growth in titanium-oxygen alloys, increasing the oxygen content in Ti-5Al-2.5Sn alloys is expected to decrease the kinetics of grain growth. At this point, it is not clear that the interstitial elements reduce the fracture toughness in alloys with only small amounts of the iron-rich second-phase present.

In order to clarify the many vague points and possible errors in the model presented above, experimental evidence is required. These experiments include completion of the work that is underway which was described previously Thin foil TEM selected area diffraction will be used to determine if α_2 has formed in the α matrix and to determine the structure of the iron-rich second-phase particles. The pole figure and texture gradient work will be completed to provide a tool to help analyze the orientation dependence of K_{Ic}. The quantitative fractography of the liquid nitrogen fracture surfaces will be completed so that the differences in fracture mode between materials and specimen type will be known without

the prejudice of the human eye. The fracture mechanism will be studied using metallographically sectioned test specimens of the Ti-5Al-2.5Sn alloys which have been plastically strained at 77°K to various levels short of final rupture. Because of the possible differences between the failure mode in tensile and K_{Ic} specimens, both types of specimens will be sectioned. Studying tensile specimens have the advantage that the deformed regions which can be observed are much larger and the macroscopic stress state is better defined than in a precracked specimen. The only K_{Ic} samples which are to be sectioned will be from the air-cooled, ELI plate. At 77°K, this was the only material which had a K_{Ic} test record with any deviation from a linear load-deflection behavior prior to fracture, and thus straining these specimens to K_{Ic} levels just short of fracture will be a less difficult experimental task. It is a good alloy to be used for comparison because it showed the greatest difference between the tensile and K_{Ic} fracture modes. Observations made on the sectioned samples will provide more detailed information about the influence of microstructure on the fracture process. To complete the description of this fracture mode, the twin systems which operate must be determined and more evidence of the presence of local order must be made. The twin system will be identified using thin foil TEM selected area diffraction. A computer program which plots the TEM diffraction patterns associated with the various twin systems in hexagonal materials[64] will be used to help identify the twin system. The determination of SRO by low angle scattering x-ray diffraction is beyond the scope of the investigation, but evidence for order can be observed by studying dislocation arrays. In a material with no SRO, dislocations within one band should be fairly evenly spaced. In an alloy with SRO present, the first two dislocations of a deformation band should be more closely spaced because of the increased stress required to destroy the local order.[63] Observations of the dislocation

arrangements will be made from thin foil TEM specimens taken from tensile specimens strained several percent at room temperature. Room temperature deformation is expected to create more dislocations and fewer twins.

B. Ti-11.5Mo-6Zr-4.5Sn (Beta III)

The model which will be used for α-aged Beta III must include explanations of why the fracture mode varies with specimen type and why the trends in K_{Ic} of metastable β titanium alloys are often opposite to the trends in tensile ductility.[49]

The fracture mode in α-aged Beta III is classical dimpled rupture. In tensile specimens, the dimples were equiaxed while in K_{Ic} specimens, there were two populations of equiaxed dimples. As suggested previously, the large dimples in both types of specimens are believed to be nucleated at primary α particles while the nucleation site of the small dimples observed on the K_{Ic} fracture surfaces are believed to be the much smaller α strengthening precipitates. The model which is given below relies heavily on the observations in aluminum alloys,[17] steels,[18] and titanium alloys[65] that voids form at the largest particles first. This seems to be independent of whether void initiation occurs by particle cracking or interface separation. In the tensile specimens of Beta III, the stress state is extremely uniform and the most likely void initiation sites are the larger primary α particles, which precipitate along the β grain boundaries. In the α-aged Beta III specimens, the plastic zone size as calculated from the finite element work of Levy, Marcal, Ostergren, and Rice[66] at the crack tip of an elastic, non-hardening plastic material is 70 μm. This is much smaller that the 125 μm β grain size which would be the spacing of the primary α on the macroscopic plane of fracture ahead of the crack. One might expect the next smallest particles, the α strengthening precipitates

which are distributed in the matrix, to act as a void nucleation site so that the crack can propagate across the β grains. Thus, in K_{Ic} specimens, two populations of dimples can be observed. The large ones nucleate along β grain boundaries and the small ones form as the crack propagates in across the β grains.

The reason that metastable β titanium alloys often have poor tensile ductilities but good fracture toughness is probably related to the difference in fracture modes. The stress required for void initiation increases with decreasing size of the void initiating particle.[17, 18] In a stress state that requires void nucleation at small particles, a toughness/ductility parameter is expected to be greater than in a stress state where the fracture mode is not directly affected by these smaller particles.

This model explains the observed phenomena in α-aged Beta III, but the assumptions used above must be shown to be valid for this alloy. An explanation for the loss of toughness in the ω-aged material must also be developed. The experimental work required to identify the fracture mechanisms in Beta III is very similar to that described for the Ti-5Al-2.5Sn alloys. For the ω-aged material, the tensile and K_{Ic} properties will be determined. Thin foil transmission electron microscopy will be used to characterize the precipitates of these alloys which are too small to be resolved in the optical microscope. Quantitative fractography will be used to clarify the difference in fracture mode with specimen type of the β+α alloy. Both tensile and K_{Ic} specimens of the α-aged material will be studied using the metallographic sectioning technique which was previously described. Based on the shape of the α-aged Beta III test record, no experimental difficulties are expected during the straining of either tensile or K_{Ic} specimens to plastic strains just short of fracture. Experimental difficulties are expected when studying the ω-aged alloy and

it is not clear at this time how the sectioning studies will be performed on this alloy.

CONCLUSIONS

The Ti-5Al-2.5Sn alloys have equiaxed α grains with an equiaxed iron-rich second-phase present. In the normal interstitial alloys, which have higher iron and interstitial contents than the extra low interstitial (ELI) alloys, the second phase has a larger size and volume fraction. The fracture toughness of the ELI alloys are always greater than those of the normal interstitial alloys and the air-cooled ELI alloys have a K_{Ic} of about 30 percent greater than the furnace cooled ELI alloys. Cooling rate from the annealing temperature had no effect on the K_{Ic} of the lower purity alloys. At 20°K (-423°F), the ELI specimens with LS orientations were tougher than the LT specimens; but no orientation effects were observed in the normal interstitial alloys. The fracture mode was dimpled rupture with both equiaxed and long, shallow dimples. Any time the K_{Ic} decreased, independent of whether it was caused by decreasing the testing temperature, higher impurity levels, or slower cooling rates, more of the fracture surface was covered by the long, shallow dimples. These features are believed to form along mechanical twin interfaces. A model was proposed based on the concept that any increase in the localized resolved shear stress acting on a twin system will increase the probability of twin nucleation which will cause more long, shallow dimples and a reduced K_{Ic}. The factors which are believed to reduce K_{Ic} include the larger size of the iron-rich second-phase particles in the normal interstitial alloys and the formation of short range order during furnace cooling. All known trends of composition, heat treatment, microstructure, and mechanical properties of equiaxed α titanium alloys fit those predicted by the model.

Solution treated Beta III (Ti-11.5Mo-6Zr-4.5Sn) had bands of what is believed to be recrystallized and non-recrystallized β. The α-aged

microstructure includes 2 μm long primary α and much smaller α aging precipitates. The fracture mode in α-aged Beta III is dimpled rupture. In tensile specimens, the dimples were of a uniform size; but the fractographs from K_{Ic} specimens showed two size populations of dimples. The nucleation of the large dimples is believed to be the primary α particles, while the small dimples are believed to form at the α strengthening precipitates. The changes in fracture mode with specimen type and the inverse behavior of tensile ductility and fracture toughness in α-aged Beta III were explained using a model based on the dimensions of the deformed regions in tensile and K_{Ic} specimens.

The models proposed for both materials need to be checked experimentally. These experiments include metallographic sectioning of tensile and K_{Ic} specimens which have been plastically strained to various levels short of fracture along with thin foil transmission electron microscopy.

ACKNOWLEDGEMENTS

This work was performed under a research grant from the National Aeronautics and Space Administration. Two members of that organization, Messrs. W. D. Klopp and W. F. Brown, Jr. have been a source of continuing help and support. The microprobe analyses of the Ti-5Al-2.5Sn alloys were performed by Professor L. F. Vassamillet. Conversations with Drs. J. C. Williams of the Rockwell Science Center and F. H. Froes of the Crucible Materials Research Center have been helpful during this investigation.

APPENDIX A

RESULTS OF INDIVIDUAL PLANE STRAIN FRACTURE TOUGHNESS TESTS

The results of the individual plane strain fracture toughness tests conducted during this investigation are listed in table form in this appendix. Data presented here satisfy the requirements of ASTM E399-74 unless otherwise noted. The requirement on fatigue crack front straightness was relaxed from 5 to 10 percent for the Ti-5Al-2.5Sn alloys. As noted previously, this does not significantly affect the ability to measure K_{Ic}.

C-2

RESULTS OF INDIVIDUAL PLANE STRAIN FRACTURE TOUGHNESS TESTS

Material: Ti-5Al-2.5Sn, ELI, Air-Cooled

Testing Conditions	Specimen Identification	Specimen Thickness B (in.)	Specimen Width W (in.)	Crack Length a (in.)	K_{Ic} (ksi$\sqrt{in.}$)	$2.5\,(K_{Ic}/\sigma_y)^2$ (in.)
295°K (72°F) σ_y=102.1 ksi Compact Tension Specimen LT Orientation	TAL-3R-6	1.002	2.000	0.947	107.9 (a, b, c)	2.793
77°K (-320°F) σ_y=173.7 ksi Compact Tension Specimens LT Orientation	TAL-1R-6	1.000	1.998	0.976	98.0	0.795
	TAL-4L-6	1.000	1.995	0.916	99.2	0.815
	TAL-6L-6	1.001	2.000	0.958	106.2	0.933
					101.1 Average	
20°K (-423°F) σ_y=189.0 ksi 1x2 Bend Specimens LT Orientation	TAL-4R-1	0.978	1.965	1.020	85.8	0.515
	TAL-5R-1	0.977	1.964	1.032	82.0	0.471
	TAL-6R-1	0.976	1.976	1.010	76.8	0.412
					81.5 Average	
20°K (-423°F) σ_y=189.0 ksi 1x1 Bend Specimens LT Orientation	TAL-4R-2	0.976	0.978	0.513	82.3	0.473
	TAL-4R-3	0.981	0.981	0.517	81.1	0.460
	TAL-5R-2	0.981	0.979	0.516	84.6	0.502
					82.7 Average	
20°K (-423°F) σ_y=189.0 ksi 1x1 Bend Specimens LS Orientation	TAL-3L-1	0.957	0.991	0.507	98.0 (b)	0.673
	TAL-3L-2	0.999	0.998	0.508	92.0 (b)	0.593
	TAL-3L-3	0.998	0.985	0.523	100.8 (b)	0.710
					96.9 (b) Average	

(a) This is not a valid K_{Ic} value because $B < 2.5\,(K_{Ic}/\sigma_y)^2$.

(b) This is not a valid K_{Ic} value because $a < 2.5\,(K_{Ic}/\sigma_y)^2$.

(c) This is not a valid K_{Ic} value because the maximum load exceeds the 5% tangent load by more than 10%.

APPENDIX A (continued)

RESULTS OF INDIVIDUAL PLANE STRAIN FRACTURE TOUGHNESS TESTS

Material: Ti-5Al-2.5Sn, ELI, Furnace Cooled

Testing Conditions	Specimen Identification	Specimen Thickness B (in.)	Specimen Width W (in.)	Crack Length a (in.)	K_{Ic} (ksi/in.)	$2.5 (K_{Ic}/\sigma_y)^2$ (in.)
295°K (72°F) σ_y=102.1 ksi Compact Tension Specimen LT Orientation	TFL-1R-6	1.000	1.995	0.916	104.9 (a, b)	2.814
77°K (-320°F) σ_y=170.6 ksi Compact Tension Specimen LT Orientation	TFL-3R-6	0.998	2.000	0.954	75.4	0.488
	TFL-6L-6	0.999	2.010	0.957	74.8	0.480
					75.1 Average	
20°K (-423F) σ_y=189.4 ksi 1x2 Bend Specimens LT Orientation	TFL-4R-1	0.977	1.964	1.013	63.7	0.282
	TFL-5R-1	0.977	1.965	1.052	65.3	0.298
	TFL-6R-1	0.977	1.963	1.019	63.1	0.277
					64.0 Average	
20°K (-423°F) σ_y=189.4 ksi 1x1 Bend Specimens LT Orientation	TFL-4R-2	0.975	0.982	0.516	64.3	0.287
	TFL-4R-3	0.965	0.980	0.494	61.0	0.259
	TFL-5R-2	0.982	0.980	0.516	60.1	0.251
					61.8 Average	
20°K (-423°F) σ_y=189.4 ksi 1x1 Bend Specimens LS Orientation	TFL-3L-1	0.994	0.997	0.519	69.1	0.333
	TFL-3L-2	0.994	0.995	0.498	74.5	0.388
	TFL-3L-3	0.998	1.000	0.504	79.3	0.439
					73.4 Average	

(a) This is not a valid K_{Ic} value because $B < 2.5 (K_{Ic}/\sigma_y)^2$.

(b) This is not a valid K_{Ic} value because $a < 2.5 (K_{Ic}/\sigma_y)^2$.

RESULTS OF INDIVIDUAL PLANE STRAIN FRACTURE TOUGHNESS TESTS

Material: Ti-5Al-2.5Sn, Normal Interstitial, Air-Cooled

Testing Conditions	Specimen Identification	Specimen Thickness B (in.)	Specimen Width W (in.)	Crack Length a (in.)	K_{Ic} (ksi/in.)	$2.5\,(K_{Ic}/\sigma_y)^2$ (in.)
295°K (72°F) σ_y=126.9 ksi	TAN-1R-6	1.001	1.998	1.028	68.5	0.729
Compact Tension Specimens	TAN-4L-6	1.000	1.989	0.956	62.2	0.600
LT Orientation					65.4 Average	
77°K (-320°F) σ_y=194.5 ksi	TAN-2R-6	1.001	1.996	0.941	50.0	0.165
Compact Tension Specimens	TAN-6L-5	0.999	1.997	0.918	47.4	0.149
LT Orientation	TAN-6L-6	1.001	2.000	0.999	48.4	0.155
					48.6 Average	
20°K (-423°F) σ_y=215.4 ksi	TAN-4R-1	0.977	1.964	1.073	47.7	0.122
1x2 Bend Specimens	TAN-5R-1	0.977	1.965	1.031	46.8	0.118
LT Orientation	TAN-6R-1	0.978	1.964	1.022	45.8	0.113
					46.8 Average	
20°K (-423°F) σ_y-215.4 ksi	TAN-4R-2	0.980	0.976	0.552	46.3	0.116
1x1 Bend Specimens	TAN-4R-3	0.980	0.978	0.563	46.9	0.119
LT Orientation	TAN-5R-2	0.976	0.978	0.540	44.9	0.108
					46.0 Average	
20°K (-423°F) σ_y=215.4 ksi	TAN-3L-1	0.999	0.998	0.530	46.0	0.114
1x1 Bend Specimens	TAN-3L-2	0.996	0.992	0.522	45.2	0.110
LS Orientation	TAN-3L-3	0.996	1.001	0.528	45.9	0.113
					45.7 Average	

APPENDIX A (continued)

RESULTS OF INDIVIDUAL PLANE STRAIN FRACTURE TOUGHNESS TESTS

Material: Ti-5Al-2.5Sn, Normal Interstitial, Furnace-Cooled

Testing Conditions	Specimen Identification	Specimen Thickness B (in.)	Specimen Width W (in.)	Crack Length a (in.)	K_{Ic} (ksi$\sqrt{in.}$)	$2.5\,(K_{Ic}/\sigma_y)^2$ (in.)
295°K (72°F) σ_y=127.9 ksi	TFN-3R-6	1.000	1.999	0.967	60.9	0.566
Compact Tension Specimens	TFN-6L-6	1.001	1.999	0.936	59.1	0.534
LT Orientation					60.0 Average	
77°K (-320°F) σ_y=200.0 ksi	TFN-1R-6	1.000	2.000	0.921	51.5	0.165
Compact Tension Specimens	TFN-4L-6	1.001	2.000	0.993	51.4	0.165
LT Orientation	TFN-6L-6	1.000	2.000	0.975	54.5	0.186
					52.5 Average	
20°K (-423°F) σ_y=220.3 ksi	TFN-5R-1	0.978	1.964	1.015	46.0	0.109
1x2 Bend Specimens	TFN-6R-1	0.977	1.964	1.016	46.3	0.110
LT Orientation					46.2 Average	
20°K (-423°F) σ_y=220.3 ksi	TFN-4R-2	0.978	0.980	0.518	42.7	0.094
1x1 Bend Specimens	TFN-4R-3	0.980	0.975	0.524	42.5	0.093
LT Orientation	TFN-5R-2	0.980	0.978	0.526	43.0	0.095
					42.7 Average	
20°K (-423°F) σ_y=220.3 ksi	TFN-3L-1	0.998	0.996	0.539	44.5	0.102
1x1 Bend Specimens	TFN-3L-2	0.997	0.986	0.515	51.1	0.135
LS Orientation	TFN-3L-3	0.995	0.996	0.527	47.9	0.118
					47.2 Average	

RESULTS OF INDIVIDUAL PLANE STRAIN FRACTURE TOUGHNESS TESTS

Material: α-Aged Beta III (Ti-11.5Mo-6Zr-4.5Sn)

Testing Conditions	Specimen Identification	Specimen Thickness B (in.)	Specimen Width W (in.)	Crack Length a (in.)	K_{Ic} (ksi$\sqrt{in.}$)	$2.5\left(K_{Ic}/\sigma_y\right)^2$ (in.)
295°K (72°F) σ_y=185.7 ksi	AC2-A1	0.750	1.504	0.763	48.4	0.170
Compact Tension Specimens	AC2-A5	0.750	1.503	0.795	50.5	0.185
LT Orientation	AC2-A11	0.750	1.502	0.775	50.4	0.184
					49.8 Average	

REFERENCES

1. R. H. Van Stone and J. R. Low, Jr., "The Effect of Microstructure on the Fracture Toughness of Titanium Alloys," NASA Technical Report No. 1-Ti, Department of Metallurgy and Materials Science, Carnegie-Mellon University, October 1974.

2. M. J. Blackburn, Trans. AIME, 239 (1967), pp. 1200-1208.

3. T. K. G. Namboodhiri, C. J. McMahon, Jr., and H. Herman, Met. Trans., 4 (1973), pp. 1323-1331.

4. C. J. McMahon, Jr. and D. J. Truax, Corrosion, 29 (1973) pp. 47-55.

5. M. J. Blackburn and J. C. Williams, Trans. ASM, 62 (1969), pp. 398-409.

6. N. E. Paton, J. C. Williams, and G. P. Rauscher, Titanium Science and Technology, Plenum Press, New York, 1973, pp. 1049-1069.

7. J. C. Williams, "A Review of the Deformation Behavior of α-Ti," presented at the Spring TMS-AIME Meeting, University of Pittsburgh, May 1974.

8. A. M. Garde, E. Aigeltinger, and R. E. Reed-Hill, Met. Trans., 4 (1973), pp. 2461-2468.

9. J. L. Christain, A. Hurlich, J. E. Chaffey, and J. F. Watson, Proc. ASTM, 63 (1963) pp. 578-597.

10. R. E. Curtis, R. R. Boyer, and J. C. Williams, Trans. ASM, 62 (1969), pp. 457-469.

11. A. W. Thompson and B. C. Odegard, Met. Trans., 4 (1973), pp. 899-908.

12. J. L. Shannon, Jr. and W. F. Brown, Jr., Proc. ASTM, 63 (1963), pp. 809-829.

13. V. C. Petersen, J. B. Guernsey, and R. C. Buehl, "Manufacturing Procedures for a New High-Strength, Beta Titanium Alloy having Superior Formability," Technical Report AFML-TR-69-171, Air Force Materials Laboratory, Wright-Patterson Air Force Base, June 1969.

14. J. C. Williams, B. S. Hickman, and D. H. Leslie, Met. Trans., 2 (1971), pp. 477-484.

15. J. A. Feeney and M. J. Blackburn, Met. Trans., 1 (1970), pp. 3309-3323.

16. J. B. Guernsey, V. C. Petersen, and F. H. Froes, Met. Trans., 3 (1972), pp. 339-340.

17. R. H. Van Stone, R. H. Merchant, and J. R. Low, Jr., Fatigue and Fracture Toughness--Cryogenic Behavior, ASTM STP 556, ASTM, Philadelphia, 1974, pp. 93-124.

18. T. B. Cox and J. R. Low, Jr., Met. Trans., 5 (1974), pp. 1457-1470.

19. D. E. Cooper, Titanium Metals Corporation of America, Toronto, Ohio, private communication.

20. L. F. Vassamillet, Carnegie-Mellon University, private communication.

21. Max Hansen, Constitution of Binary Alloys, McGraw-Hill, New York, 1958, pp. 1210-1214.

22. Francis A. Shunk, Constitution of Binary Alloys, Second Supplement, McGraw-Hill, New York, 1969, pp. 351-352.

23. R. D. Schoone and E. A. Fiscione, Rev. Sci. Instruments, 37 (1966), pp. 1351-1553.

24. M. J. Blackburn and J. C. Williams, Trans. AIME, 239 (1967), pp. 287-288.

25. B. S. Hickman, Trans. AIME, 245 (1969) pp. 1329-1336.

26. Sam Leber, Rev. Sci. Instruments, 36 (1965), pp. 1747-1750.

27. S. L. Lopata and E. B. Kula, Trans. AIME, 224 (1962), pp. 865-866.

28. R. H. Olsen, Metallography, 5 (1972), pp. 369-371.

29. R. H. Olsen and W. D. Smith, Metallography, 4 (1971), pp. 515-520.

30. A. J. Hatch, Trans. AIME, 233 (1965), pp. 44-50.

31. Frank Larson and Anthone Zarkades, "Properties of Textured Titanium Alloys," Metals and Ceramics Information Center Report MCIC-74-20, Battelle, Columbus, Ohio, June 1974.

32. D. Lee and W. A. Backofen, Trans. AIME, 236 (1966), pp. 1696-1704.

33. Adam A. Neville and John B. Kennedy, Basic Statistical Methods for Engineers and Scientists, International Textbook, Scranton, Pa., 1964, pp. 143-150.

34. F. H. Froes, Colt Industries, Crucible Materials Research Center, Pittsburgh, Pa., private communication.

35. J. L. Shannon, Jr., "NASA-Lewis' Facilities and Techniques for Fracture Toughness Tests in Liquid Hydrogen," presented at Materials Testing and Quality Control Show and Conference, Detroit, Michigan, October, 1974.

36. J. L. Shannon, Jr., NASA Lewis Research Center, Cleveland, Ohio, unpublished research.

37. George E. Dieter, Jr., Mechanical Metallurgy, McGraw-Hill, New York, 1961, pp. 243-247.

38. P. W. Bridgman, Studies in Large Plastic Flow and Fracture, McGraw-Hill, New York, 1952, pp. 1-37.

39. S. N. Monteiro and R. E. Reed-Hill, Met. Trans., 4 (1973), pp. 1011-1015.

40. "Standard Method of Test for Plane-Strain Fracture Toughness of Metallic Materials," ASTM Designation E399-74, 1974 Book of ASTM Standards, Part 31, 1974, pp. 432-451.

41. J. G. Kaufman, Alcoa Technical Center, Alcoa Center, Pa., private communications.

42. Adam A. Neville and John B. Kennedy, Basic Statistical Methods for Engineers and Scientists, International Textbook, Scranton, Pa., 1964, pp. 171-182.

43. J. G. Kaufman, F. G. Nelson, and R. H. Wygonik, Fatigue and Fracture Toughness--Cryogenic Behavior, ASTM STP 556, ASTM, 1974, pp. 125-158.

44. E. B. Kula and T. S. DeSisto, Behavior of Metals at Cryogenic Temperatures, ASTM STP 387, ASTM, 1966, pp. 3-31.

45. H. Conrad, K. Okasaki, V. Gadgil, and M. Jon, Electron Microscopy and Structures of Materials, University of California Press, Berkeley, California., 1972, pp. 438-469.

46. J. R. Low, Jr., Prog. Mat. Sci., 12 (1963), pp. 1-37.

47. R. J. H. Wanhill, Acta Met., 21 (1973), pp. 1253-1258.

48. J. C. Williams, Rockwell Science Center, Rockwell International, Thousand Oaks, California, private communications.

49. F. H. Froes, R. F. Malone, V. C. Petersen, C. G. Rhodes, and J. C. Williams, "Research on Deep Hardening Titanium Alloy for Large Airframe Structural Members," Report IR 7351 (V), Air Force Materials Laboratory, Wright-Patterson Air Force Base, Ohio, 1973.

50. J. C. Chesnutt and J. C. Williams, Scanning Electron Microscopy/1974 (Part IV), IIT Research Institute, 1974, pp. 895-902.

51. R. E. Reed-Hill, Deformation Twinning, Gordan and Breach, New York, 1964, pp. 295-320.

52. J. N. Goodier, J. App. Mech., Trans. ASME, 55 (1933), pp. 39-44.

53. R. H. Edwards, J. App. Mech., Trans. ASME, 18 (1951) pp. 19-30.

54. M. F. Ashby, Phil. Mag., 14 (1966), pp. 1157-1178.

55. E. F. Erbin, Proc. ASTM, 63 (1963), pp. 826-827.

56. P. A. Flinn, Strengthening Mechanisms in Solids, ASM, 1962, pp. 17-50.

57. M. J. Blackburn and J. C. Williams, Trans. ASM, 62 (1969), pp. 398-409.

58. Rodney P. Elliott, Constitution of Binary Alloys, First Supplement, McGraw-Hill, New York, 1965, pp. 555-556.

59. A. Munster and K. Sagel, The Physical Chemistry of Metallic Solutions and Intermetallic Compounds, Volume 1, Her Majesty's Stationery Office, London, 1959, Paper 2D.

60. H. R. Ogden, D. J. Maykuth, W. L. Finlay, and R. I. Jaffee, J. Metals, 5 (1953), pp. 267-272.

61. R. W. Cahn, Local Atomic Arrangements Studied by X-Ray Diffraction, Gordon and Breach, New York, 1966, pp. 179-214.

62. P. P. Dessau and C. L. Harris, "Premium Quality 5Al-2.5Sn ELI Titanium Production," NASA-CR-132227, Final Report, Aerojet Nuclear Systems Company, Azusa, Cal., May 1972.

63. S. Mahajan and D. F. Williams, Met. Rev., 18 (1973), pp. 43-61.

64. Robert J. DeAngelis, Met. Trans., 5 (1974), pp. 520-521.

65. M. A. Greenfield and H. Margolin, Met. Trans., 3 (1972), pp. 2649-2659.

66. N. Levy, P. V. Marcal, W. J. Ostergren, and J. R. Rice, Int. J. Frac. Mech., 7 (1971), pp. 143-156.